Title: Immune–tracheal intercellular signalling coordinates the muscle injury response in *Drosophila*

Authors: Nourhene Ammar[1], Olivier Josse[1], Aurélien Guillou[1], Jessica Perochon[2] and Hadi Boukhatmi[1]*

[1] Institut de Génétique et Développement de Rennes (IGDR), Université de Rennes, CNRS UMR6290, Rennes, France.

[2] Institute of Cancer Sciences−University of Glasgow, Wolfson Wohl Cancer Research Centre, Glasgow, UK.

* Corresponding author: hadi.boukhatmi@univ-rennes.fr

Summary

Effective tissue adaptation to damage requires precise coordination among diverse cell types. In skeletal muscle, injury-responsive cells play a pivotal role in repair, yet the molecular and cellular mechanisms governing their coordinated activity remain incompletely understood. Here, we identify adult *Drosophila* immune cells-hemocytes-as key mediators of the muscle injury response. Following damage, hemocytes are rapidly recruited to affected fibers, where they perform dual functions. First, they promote tracheal (respiratory cell) branching by depositing the FGF ligand Branchless (Bnl) along damaged muscle, which activates its receptor, FGFR/Breathless (Btl), on tracheal cells, stimulating their outgrowth toward the injury and supporting oxygen delivery. Second, hemocytes contribute to structural stabilization by supplying key extracellular matrix (ECM) components, including SPARC and Collagen IV, to the damaged fiber. Together, these findings uncover a coordinated injury response in which immune cells act as central mediators of metabolic and structural adaptation in response to damage.

Introduction

Effective tissue repair relies on a complex interplay requiring precise communication and coordination between cells across multiple tissues and organ systems (Sun and Poss, 2023). Disruption of these interactions can impair regeneration and, in severe cases, threaten organismal survival (Li et al., 2016). In mammals, skeletal muscle regeneration, in particular, depends on a tightly orchestrated collaboration among various cell types, including macrophages, muscle stem cells (MuSCs, also known as satellite cells), and fibro/adipogenic progenitors (FAPs) (Relaix et al., 2021). For example, following muscle injury, macrophages signal to MuSCs to regulate their proliferation and subsequent differentiation to restore damaged muscle fibers (Dort et al., 2019). Simultaneously, the vascular system is mobilized to meet increased metabolic demands and to support the structural remodelling of damaged tissue (Eming et al., 2014). Despite these insights, the signalling events that coordinate cellular recruitment and tissue adaptation in response to muscle damage remains poorly understood.

Like many organisms in the wild, *Drosophila* frequently encounters natural wounding, requiring efficient tissue adaptation mechanisms to maintain function and ensure survival (Subasi et al., 2024). *Drosophila* has long served as a powerful model for studying myogenesis (Laurichesse and Soler, 2020), and more recently, it has emerged as an effective system for investigating adult muscle response to injury (Boukhatmi, 2021; Catalani et al., 2022; Chaturvedi et al., 2017; Goh et al., 2024; Gunage et al., 2017). Although much attention has focused on the role of *Drosophila* MuSCs in regeneration, relatively little is known about how other cell types contribute to muscle adaptation to damage. In particular, the contribution of the immune blood cells-hemocytes-remains largely unexplored. Despite limited hematopoiesis in adults, hemocytes are essential for detecting and responding to bacterial infections (Sanchez Bosch et al., 2019). Approximately 85% of adult hemocytes are plasmatocytes, macrophage-like cells that are distributed throughout the body (Boulet et al., 2021). Studies, including our own, have shown that they can populate the indirect flight muscles (IFMs) under normal conditions (Boukhatmi and Bray, 2018; Sanchez Bosch et al., 2019). However, whether these immune cells engage in active intercellular signalling following muscle damage, and how they coordinate with other cell types, remains an open question.

The tracheal cells -a network of air-filled tubes that functions analogously to the vertebrate vascular and respiratory systems- enwrap and penetrate muscle fibers to oxygenate them (Sauerwald et al., 2019). These connections are established during development through the Branchless (Bnl) FGF pathway (Peterson and Krasnow, 2015). The *Drosophila* FGF ligand Branchless (Bnl), produced by muscle cells, directs tracheal migration by activating the Breathless (Btl) receptor on tracheal cells. For decades, tracheal branching has been well characterized at the morphological, cellular, and genetic levels during *Drosophila* development (Ebner et al., 2002; Ghabrial et al., 2003; Hayashi and Kondo, 2018; Rao et al., 2015). More recently, it has been shown that the adult trachea also undergoes dynamic remodelling to sustain adult gut regeneration (Perochon et al., 2021; Tamamouna et al., 2021), raising the possibility that similar remodelling could contribute to muscle responses following injury. In addition, hemocytes have been shown to closely associate with adult tracheal cells (Sanchez Bosch et al., 2019). However, whether hemocytes and tracheal cells cooperate to mediate a coordinated response to muscle damage remains to be studied.

In this study, we investigated how intercellular communication between muscles, hemocytes, and tracheal cells coordinates the response to muscle injury in adult *Drosophila*. We found that both physical and genetically induced muscle damage trigger the immediate and sustained recruitment of hemocytes to injured fibers. This recruitment is essential for directing tracheal remodeling via Bnl/Btl signaling, enabling the selective identification of damaged fibers over intact ones. Beyond their role in tracheal guidance, hemocytes also contribute to muscle maintenance and repair by producing extracellular matrix (ECM) components. Together, these findings reveal a coordinated injury response in which immune cells act not merely as passive responders, but as central mediators of both signaling and structural adaptation during the early stages of muscle recovery.

Results

Hemocytes are specifically recruited to the injured adult flight muscle

Although *Drosophila* is one model organism for studying muscle repair, it lacks molecular markers that reliably and specifically identify injured muscle fibers. In vertebrates, the re-expression of embryonic myosin heavy chain (MyHC-emb) in damaged fibers is a common marker of muscle injury and regeneration (Murphy et al., 2011). To assess whether Myosin Heavy Chain (Mhc) expression could similarly serve as an indicator of muscle damage in *Drosophila*, we analysed its expression following injury. Our results show that Mhc expression is drastically upregulated in injured muscles and inversely correlated with the downregulation of Mef2, providing a robust molecular readout of muscle damage (Figure 1 A-F and G; Figure S1 A-B''). This upregulation persists for at least 20 days post-injury (DPI) (Figure S2 E-N). In *Drosophila*, several Mhc isoforms are generated via alternative splicing of a single *Mhc* gene (Orfanos and Sparrow, 2013). To determine which isoform respond to injury, we analysed the expression of various GFP-tagged Mhc isoforms (Orfanos and Sparrow, 2013; Sarov et al., 2016). Only the shorter adult Mhc isoforms-K, L, and M-were upregulated in response to muscle damage (Figure S1 C-E). To rule out the possibility that Mhc upregulation is an artifact of the injury method used, we examined its expression in *Naa30* mutants, which exhibit developmental defects in flight muscles and spontaneous muscle detachment in eight-day-old adults, along with loss of nuclear Mef2 expression (Varland et al., 2023). In these mutants, Mhc upregulation coincided with Mef2 downregulation (Figure 1 I-J'''; Figure S1 F-G''), further supporting Mhc as a reliable marker of muscle damage in *Drosophila*.

To study the hemocytes response to IFMs damage, we started by tracking these cells at various time points after injury using the hemocytes reporters Peroxidasin (*Pxn*) (Figure 1 A-C'') and Hemolectin (*Hml*) (Figure S1 H-I'). Co staining for these markers and Mhc revealed extensive recruitment of hemocytes to the injured muscle fibers (Figure 1 A-C'; Figure S1 H-I'). Notably, while Pxn+ hemocytes persist at the injured muscle for at least 5 DPI, Hml+ hemocytes enrichment declines over time (Figure 1 H'), highlighting the heterogeneity of the adult hemocyte population, consistent with previous findings (Boulet et al., 2021). To further characterize the hemocytes

recruitment dynamics, we examined the transcription factor Zfh1 and its reporter (*Enh3-Gal4 > UAS-mCD8GFP*), another hemocytes marker (Boukhatmi and Bray, 2018; Wu et al., 2019) (Figure 1 D-F''; Figure S2 A-B'). Enh3+ hemocytes exhibited recruitment kinetics similar to Pxn+ cells (Figure 1 H'). Importantly, at 5 DPI all Pxn+ cells were also Enh3+, whereas only a subset of Pxn+ cells were Hml+ (Figure 1 H and Figure S1 H-M'). None of the recruited hemocytes expressed Mef2 (Figure S1 L'-M'). To confirm that hemocytes recruitment is a response to muscle damage, we analyzed *Naa30* mutants. Consistently, we observed a selective recruitment of Enh3+ hemocytes to injured muscle fibers, identified by high Mhc expression and the loss of Mef2 nuclear expression (Figure 1 I-J'''). Altogether, these data show that adult hemocytes are rapidly and specifically recruited to injured muscle fibers, with distinct subpopulations displaying differential persistence over time.

Hemocytes recruitment coordinates with tracheal remodeling following muscle injury

The selective recruitment of hemocytes to damaged fibers suggests a potential role in the muscle damage response. We observed that hemocytes within the indirect flight muscles (IFMs) are closely associated with tracheal cells (Figure 2 A-A'). It has previously been shown that tracheal cells can extend new branches toward damaged regions to support adult gut regeneration (Perochon et al., 2021; Tamamouna et al., 2021). We therefore asked whether tracheal remodelling also occurs in response to IFMs injury and whether it could be functionally linked to hemocyte recruitment. Our analysis revealed that muscle damage, whether caused by physical injury or in *Naa30* mutant animals, leads to a significant increase in tracheal coverage of the injured fiber (Figure 2 B-D and Figure S2 C-D'). The invasion is directed toward the injury site, with the highest branching density near the damaged area and progressively decreasing with distance from the injury (Figure 2 E). We further observed that hemocytes remain spatially close to the tracheal branches, even under injured conditions (Figure 2 C'').

To further investigate the tracheal response to injury, we focused on terminal tracheal cells (TTCs), specialized branches of the tracheal system known for their structural plasticity and ability to invade tissues, including muscle fibers, to deliver oxygen (Ghabrial et al., 2003; Peterson and Krasnow, 2015; Sauerwald et al., 2019). TTCs can be reliably identified by their distinctive morphology and the expression of the

transcription factor Serum Response Factor (dSRF) (Figure 2 F-F' and J-J'). We visualized TTCs by expressing membrane-bound GFP under the control of dSRF-Gal4 (*dSRF-Gal4 > UAS-mCD8GFP*) (Figure 2 G-H'''). We observed a high density of TTCs within injured muscle fibers, with the highest concentration near the injury site (Figure 2 H-H''' and I). Orthogonal views showed that the recruited tracheae are found not only on the muscle surface but also extend branches into the injured fibers (Figure 2 G'''-H'''), consistent with the atypical muscle–tracheal organization optimized to deliver oxygen deep within the muscle, directly to sites of high metabolic demand (Peterson and Krasnow, 2015; Sauerwald et al., 2019). Labelling TTCs nuclei with anti-dSRF confirmed the significant enrichment of dSRF+ nuclei along the injured fibers comparing to the uninjured muscles (Figure 2 K-L'' and M). The tracheal enrichment at the injured muscle results from TTCs branching rather than proliferation, as no PH3+ cells were detected in the muscle trachea cells (Figure 2 K'''-L'''). Altogether, these data indicate that tracheal cells respond to muscle injury and target specifically the damaged fiber.

We found that tracheal remodelling is irreversible, as tracheal enrichment at the injured muscle persists even 20 days post-injury (Figure S2 E-M' and P), a time point when muscle healing is expected to be complete (Catalani et al., 2022; Chaturvedi et al., 2017). A comparison of hemocyte recruitment kinetics with tracheal coverage density revealed that hemocyte recruitment precedes tracheal coverage of the injured fibers (Figure S2 O and P), raising the possibility of an interplay between the two-cell population in supporting the injured muscle fiber.

Tracheal invasion of injured muscle fibers is triggered by local hypoxia

The tracheal recruitment to injured muscle fibers (Figure 2) suggests a critical oxygen demand of the damaged muscle. If this is the case, local hypoxia within injured fibers should serve as a key cue for tracheal attraction and directional growth toward the site of injury, as seen in other physiological contexts (Jarecki et al., 1999). To assess oxygen variations within the injured muscle, we first used the Synthetic HRE (Hypoxia response element) nuclear sensor (SyHREns), a hypoxia reporter that serves as a proxy for evaluating intracellular oxygen fluctuations (Zhao et al., 2024). The SyHREns was found to be expressed in some TTCs, which are identifiable by both their triangular

shape and expression of dSRF, in normal conditions (Figure 3 A-A''). Importantly, we observed a pronounced enrichment of SyHREns-positive cells surrounding injured muscle fibers, in close proximity to the recruited tracheal branches (Figure 3 B-D''). The number of SyHREns+ cells around the injured fibers remained stable for at least 20 DPI (Figure 3 E), indicating that local hypoxia persists in parallel with the sustained tracheal remodelling observed over the same period.

In *Drosophila*, as in mammals, hypoxia-induced tracheogenesis is controlled by the transcription factor Similar (Sima) -the *Drosophila* homolog of hypoxia-inducible factor-1α (HIF-1α)- a central regulator of hypoxic and angiogenic responses (Jarecki et al., 1999)). Accordingly, silencing *sima* in TTCs prevented tracheal expansion towards the injured fibers (Figure 3 F-I). Bnl is a well-established downstream effector of hypoxic signalling, deposited locally on hypoxic tissues to promote tracheal attraction (Jarecki et al., 1999). We therefore hypothesised that if the injured muscle undergoes hypoxia, Bnl should accumulate locally at the damaged fiber to facilitate tracheal remodelling. Analysing the expression of an endogenously tagged *Bnl:GFP*^{endo} allele (Du et al., 2018) revealed marked enrichment of Bnl at injured muscle fibers compared to adjacent intact ones (Figure 3 J-L). Altogether, these data suggest that muscle damage induces local muscle oxygen starvation, which in turn drives tracheal cell recruitment to the injured tissue.

Hemocytes deposit Bnl/FGF at injured muscles to mediate tracheal recruitment

During both embryonic and post-embryonic stages, tracheal guidance is regulated in a dose-dependent manner by local Bnl concentrations (Jarecki et al., 1999). In adult flight muscle development, muscle-tracheal connections are established through the action of Bnl, which is secreted by muscle fibers and acts in a paracrine manner by binding to its receptor, FGFR/Breathless (Btl), expressed on tracheal cells (Peterson and Krasnow, 2015). The observed enrichment of Bnl in injured muscles (Figure 3 J-K) raises two key questions: Is Bnl/Btl signaling functionally involved in directing tracheal recruitment to damaged fibers? If so, what is the source of Bnl enrichment on the injured fibers? To begin addressing these questions, we conditionally overexpressed Bnl in a restricted subset of adult muscle fibers using the flip-out system combined with a regionally expressed driver (Figure S3 A-C and Materials and Methods section). This targeted overexpression was sufficient to recruit tracheal cells

to the ectopic Bnl-expressing regions (Figure 4 A–C'), and did so in a dose-dependent manner: higher levels of Bnl expression (5 days) resulted in more pronounced tracheal remodeling compared to lower expression (24 hours). These findings demonstrate that the adult tracheal system remains responsive to elevated Bnl levels in the IFMs, supporting the hypothesis that Bnl/Btl signaling directs tracheal pathfinding in response to muscle injury.

We next sought to identify the cellular source responsible for Bnl accumulation in injured muscle fibers. Under wild-type conditions, Bnl:GFP^{endo} signal was detected in hemocytes, tracheal cells, and indirect flight muscles (IFMs) (Figure 4 D-D'). However, since Bnl is a diffusible protein, these observations alone cannot distinguish between cells that produce Bnl and those that merely take it up. To address this, we used the *bnl-lacZ* transcriptional reporter, which revealed active *bnl* expression in hemocytes, adult IFMs, and terminal tracheal cells (TTCs), confirming that these cell types are bona fide sources of Bnl under homeostatic conditions (Figure 4 E-F'). Given that canonical Bnl/Btl signaling operates in a paracrine manner, injured muscles and hemocytes emerge as the most plausible sources of injury-induced Bnl accumulation. To distinguish between these two possibilities, we examined *Bnl-lacZ* expression following injury. Surprisingly, we found that injured fibers lacked *Bnl-lacZ* activity, whereas neighboring uninjured fibers retained its expression (Figure S3 D-E''). These findings indicate that the injured muscle fibers themselves do not contribute to the localized Bnl accumulation after injury and suggest that the source of Bnl is extrinsic to the damaged tissue.

By contrast, we observed a marked enrichment of Bnl:GFP^{endo} signal surrounding Pxn+ hemocytes recruited to the damaged fibers, suggesting that hemocytes might be responsible for Bnl deposition along the injured muscle (Figure 4 G-H''). To functionally assess the contribution of hemocyte-derived Bnl to tracheal invasion, we selectively silenced *bnl* in hemocytes using either the *Enh3-Gal4* or *HmlΔ-Gal4* drivers. While hemocyte recruitment to the injured muscle remained unaffected, *bnl* knockdown significantly impaired tracheal invasion into damaged fibers compared to controls (Figure 4 I-M; Figure S3 F-I). Together, these results show that hemocytes infiltrating injured muscle tissue act as a key source of Bnl, which is essential for tracheal recruitment.

The receptor FGFR/Btl is essential for injury-induced tracheal guided outgrowth

The finding that Bnl orchestrates tracheal morphogenesis in response to muscle damage suggested in turn that it activates its receptor Btl, on tracheal cells, thereby driving guided outgrowth and branching. To investigate this, we examined Btl expression in adult flight muscles using an endogenously tagged *Btl:cherry*^{endo} allele, which faithfully reports Btl expression (Du et al., 2018). Btl:cherry^{endo} was detected along tracheal branches under homeostatic conditions and within tracheal structures invading the injured muscle (Figure 5 A-B''). To complement this approach, we expressed a membrane-tethered GFP (mCD8-GFP) under the control of a *Btl-Gal4* driver (Figure 5 C-E). While Btl:cherry^{endo} reflects consistent endogenous expression, *Btl-Gal4* drives a more heterogeneous pattern across tracheal cells (Figure 5 C-C'). Nevertheless, we observed a striking accumulation of tracheal branches labelled by *Btl-Gal4* at injured muscles, reinforcing that Btl-expressing tracheal cells are actively recruited to damaged fibers (Figure 5 D-E). We then tested whether Btl function is required for proper tracheal pathfinding. To this end, *btl* was specifically silenced in tracheal cells using either *dSRF-Gal4* or *btl-Gal4* drivers (Figure 5 F-I''). In both cases, tracheal invasion into injured fibers was significantly impaired compared to the control (Figure 5 J). Notably, the phenotype was more pronounced when using *dSRF-Gal4*, which is expected given its broader and more uniform expression pattern in terminal tracheal cells (Figure 2 F and G) compared to *Btl-Gal4*. Together, these findings showed that the Bnl/Btl signaling axis plays a pivotal role in guiding tracheal remodeling after muscle damage. While Btl expression is restricted to tracheal cells, localized Bnl secretion from hemocytes at the damaged fiber refines tracheal pathfinding, ensuring precise and targeted tracheal invasion into injured muscle.

Hemocytes supply ECM components to adult muscles

The extracellular matrix (ECM) is critical for muscle repair, providing structural support, mediating cell signalling, and facilitating tissue remodelling (Schuler et al., 2022). Hemocytes are known to be major producers of ECM components during both *Drosophila* development and post-developmental stages (Bunt et al., 2010; Gold and Bruckner, 2015). Based on this, we hypothesized that they might also supply key ECM

components in response to adult muscle injury. Collagen IV, a principal structural protein of the muscle ECM, plays a vital role in maintaining muscle integrity in both *Drosophila* and vertebrates (Borchiellini et al., 1996). We analysed Collagen IV distribution in adult flight muscles using the Vkg::GFP line (Figure 6 A-B''). Under homeostatic conditions, we detected a basal level of Vkg::GFP surrounding muscle fibers and along tracheal branches (Figure 6 A'). We further found that hemocytes express Collagen IV (Figure 6 A''). Five days after injury, Vkg::GFP is much more abundant in damaged fibers compared to the intact muscles and the controls (Figure 6 A-B and A''-B''). To further assess the relationship between hemocytes and ECM remodeling, we examined Collagen IV distribution at multiple time points post-injury (From 1 to 20DPI) and compared it to the pattern of hemocytes recruitment (Figure 6 C-H). The results show that the more evenly hemocytes are distributed along the injured fiber, the more abundant Vkg::GFP is detected along the same region. These observations show a correlation between Collagen IV accumulation at injured muscles and the presence of newly recruited hemocytes, raising the possibility that hemocytes may contribute to ECM remodelling in response to muscle injury.

Given that the incorporation of Collagen IV into the ECM requires accessory molecules for proper deposition and stabilization, we next investigated whether hemocytes also supply such regulatory components. One such regulator is SPARC, a collagen-binding glycoprotein essential for Collagen IV diffusion, stabilization, and incorporation into basement membranes (Bradshaw, 2009; Chioran et al., 2017). We first examined SPARC localization in hemocytes associated with adult flight muscles. Hemocytes identified using either *Enh3-Gal4* or *HmlΔ-Gal4* drivers were positive for SPARC (Figure 6 I-I' and J-J'). Importantly, when muscle is injured, SPARC was found at higher levels along the injured fiber compared to the controls, mimicking the distribution of Collagen IV (Figure 6 K-K'). These observations suggest that, in adult muscle, SPARC is locally produced by hemocytes. To further confirm the cellular source of SPARC in adult flight muscles, we used the *SPARC-Gal4* driver a Gal4 trap line inserted into the endogenous SPARC locus to drive membrane-targeted RFP (myr-RFP) expression in flies also carrying a BM40-SPARC-GFP fosmid reporter (Figure 6 L-L'). This dual-reporter approach allowed us to simultaneously visualize SPARC (via BM40-SPARC-GFP) and identify the specific SPARC-producing cells (via *SPARC-Gal4 > myr-RFP*), thereby determining whether SPARC is produced by hemocytes at the site of injury. In

uninjured muscle, BM40-SPARC-GFP and SPARC-Gal4-driven myr-RFP were co-expressed in hemocytes. Following muscle injury, BM40-SPARC-GFP was broadly enriched along the damaged fiber, resembling the distribution of endogenous SPARC protein, while *SPARC-Gal4* activity remained restricted to hemocytes and was not detected in muscle nuclei (Figure 6 M-M'). Together, these data show that recruited hemocytes are the primary source of SPARC at the injured muscle fiber.

We then sought to determine whether hemocyte-derived SPARC is required for adult muscle homeostasis. Detailed analysis of hemocytes distribution within the indirect flight muscles revealed that, in addition to their enrichment near tracheal structures, hemocytes are also concentrated at fiber tips (Figure 6 N-N' and (Boukhatmi and Bray, 2018)). Given that the extracellular matrix (ECM) is essential for the development and function of myotendinous junctions (Chu and Hayashi, 2021), we hypothesized that hemocyte enrichment at muscle tips may support muscle attachment through local ECM deposition. To test this, we specifically depleted *sparc* in hemocytes by expressing $Sparc^{RNAi}$ under the control of the *Enh3-Gal4* driver (*Enh3-Gal4 > UAS-*$Sparc^{RNAi}$). Notably, targeted downregulation of *sparc* in hemocytes for seven days resulted in pronounced muscle damage, particularly at the fiber tips adjacent to the myotendinous junctions, as evidenced by increased Mhc expression and muscle architecture disruptions (Figure 6 O-Q). Thus, the morphological defects observed upon *sparc* depletion align with this spatial distribution, supporting a functional role for hemocyte-derived Sparc in maintaining adult muscle structural integrity.

Discussion

Our study provides a compelling example of how the muscle damage response relies on the precise coordination between multiple cell types. While *Drosophila* hemocytes are traditionally recognized for their immunoprotective roles against pathogens and infections (Gold and Bruckner, 2015; Kalra et al., 2018; Sanchez Bosch et al., 2019), our findings reveal that they also play essential roles for preserving adult muscle integrity. We show that hemocytes both signal to the tracheal system to finely regulate its outgrowth toward the injured muscle and directly supply key extracellular matrix (ECM) components to the damaged fiber -two processes that likely support muscle structural maintenance and recovery (Figure 7).

A functional cooperation between immune cells and the respiratory system

Insect respiration has traditionally been viewed as entirely dependent on the tracheal system, operating independently of blood cells. However, this view has been challenged by recent finding showing that a subtype of larval hemocytes, known as crystal cells, can take up oxygen from tracheal cells and contribute to tissue oxygenation (Shin et al., 2024). We found that adult hemocytes are in close proximity with tracheal cells in muscle tissue and contribute indirectly to oxygen delivery by guiding tracheal branches toward sites of muscle injury (Figure 7). Following damage, hemocytes are rapidly recruited and cover the injured muscle. In this context, they secrete key signalling cues-specifically through the FGF/FGFR (Bnl/Btl) pathway-that promote local tracheal outgrowth and precise positioning, thereby supporting oxygenation of the damaged tissue. Interestingly, during development, plasmatocytes have been shown to transdifferentiate into crystal cells in the lymph gland, the primary hematopoietic organ (Marcetteau et al., 2025). Whether a similar transdifferentiation occurs in the adult following muscle injury remains an open question. Finally, the nature of the signals that govern hemocyte recruitment under injury conditions also remains an important avenue for future investigation.

Do Drosophila repair or regenerate their flight muscles?

The IFMs generate the high-frequency wing beats that enable flight -a behavior essential for predator avoidance, foraging, and mating. Given their vital function, IFMs must be maintained in optimal condition to ensure sustained performance throughout the animal's lifespan. This need for resilience is also underscored by the observation that over 30% of wild-caught *Drosophila* exhibit wound injuries, frequently located in the thorax and abdomen (Subasi et al., 2024). Although a rare population of satellite-like cells has been identified in adult flies, the regenerative capacity of adult *Drosophila* muscles remains debated (Chechenova et al., 2024). A major limitation has been the lack of appropriate molecular markers to monitor both muscle regeneration and muscle stem cell (MuSC) activity. In our study, we identified Myosin Heavy Chain (Mhc) as a robust marker that is consistently upregulated in damaged fibers. However, unlike in vertebrates -where MyHC-emb levels return to baseline following regeneration- Mhc

expression in *Drosophila* remains elevated even 20 days post-injury (Figure S2). This makes Mhc a sensitive marker for identifying injury, but less useful for assessing complete muscle recovery. Adult MuSCs have been identified via the transcription factor Zfh1/ZEB and its reporter Enh3 (Boukhatmi and Bray, 2018; Chaturvedi et al., 2017), which currently stands as the only known marker for these cells. An equivalent role of ZEB was recently shown in mice (Siles et al., 2019). Interestingly, both Zfh1 and ZEB are expressed in the muscle associated immune cells (Boukhatmi and Bray, 2018; Siles et al., 2019), underscoring the evolutionary conservation of this transcriptional regulator. In our study, we found that following muscle injury, 100% of the cells recruited to damaged fibers are both Enh3$^+$ and Pxn$^+$ (a plasmatocytes marker), while being negative for the muscle-specific marker Mef2 (Figure S1 L-M'). This strongly suggests that hemocytes are the predominant -if not exclusive- cell population migrating to injured muscle. These findings suggest that adult *Drosophila* flight muscles possess limited regenerative capacity and may instead rely on compensatory mechanisms-such as increased oxygenation through tracheal remodelling and structural reinforcement via extracellular matrix (ECM) deposition-to cope with muscle damage. This is consistent with the broader idea that short-lived species prioritize immediate survival and reproduction over long-term regenerative investment (Kirkwood, 2005). In such organisms, evolution favors fast and efficient repair mechanisms that support rapid recovery and fitness over complex, energy-intensive regeneration programs.

Functional parallels between Drosophila hemocytes and mammalian FAPs

In mammals, extracellular matrix (ECM) remodeling is essential for maintaining muscle structure and enabling proper tissue repair. Although muscle stem cells (MuSCs) can produce some ECM components (Baghdadi et al., 2018), the primary contributors to ECM production and maintenance during regeneration are fibro-adipogenic progenitors (FAPs) (Molina et al., 2021). *Drosophila* lack dedicated FAPs, raising the question of how flies achieve ECM remodeling and maintain muscle integrity. During development, hemocytes are the primary source of ECM molecule production (Gold and Bruckner, 2015; Mase et al., 2021; Shahab et al., 2015). However, direct functional evidence for their involvement in ECM remodeling in adult tissues—particularly muscle—has remained limited. Here, we showed that adult hemocytes produce at least two key ECM components -Collagen IV and SPARC. This production is

particularly enriched around damaged muscle fibers where hemocytes are abundant. We further showed that hemocyte-specific ablation of SPARC led to muscle deffect, indicating that hemocyte-derived ECM is essential for proper muscle architecture safeguard. We speculate that the ECM produced along the injured muscle by the hemocytes may serve not only to stabilize the tissue but also to restrict the diffusion of key signalling molecules such as Bnl, potentially confining them to the injury site and enhancing their local action. These findings suggest that *Drosophila* hemocytes share functional similarities with mammalian FAPs and may compensate for their absence. This highlights an evolutionarily flexible strategy for achieving tissue repair in organisms with fewer specialized cell types.

Materials and Methods

Drosophila melanogater strains and genetics

All *Drosophila melanogaster* stocks were grown on standard medium at 25°C. The following stains were used: w^{118} as wild type (wt), *Pxn-RFP* (Rodrigues et al., 2021), *HmlΔ-Gal4* (BL#30140), *Enh3-Gal4* (Boukhatmi and Bray, 2018), *Mhc-Iso-K, L, M (fTRG500)* and *Mhc-Iso-A, F, G (fTRG519)* (Sarov et al., 2016), *weeP26* (Orfanos and Sparrow, 2013), *Bnl:GFP*^{endo} *and Btl:cherry*^{endo} (Du et al., 2018), *Bnl-LacZ* (BL#11704), , *dSRF-GAL4* (BL#25753), *Btl-Gal4* (BL#78328), *UAS-Btl*^{RNAi} (BL#435544), *UAS-Bnl*^{RNAi} (BL#34572), *UAS-Bnl::GFP* (Lin, 2009), *Vkg::GFP* (BL#98343), *BM40-SPARC-GFP* (Sarov et al., 2016), *SME-Gal4* (VT 0576871), *UAS-H2B-RFP* (Antonello et al., 2015), *UAS-mCD8GFP* (BL#5137), *UAS-myr-mRFP* (BL#7118), SyHREns (Zhao et al., 2024), *UAS-Sima*^{RNAi} (BL#26207), *SPARC-Gal4* (BL#77473), *UAS-SPARC*^{RNAi} (BL#40885). *Naa30A* deletion males were obtained from crosses between *Naa30A*$^{\Delta 74}$*/FM0* females and either UAS-mCD8GFP; Enh3-Gal4 (Figure 1) or Mhc-Iso-K, L, M (Figure S1) males. RNAi experiments were carried out at 29°C. To achieve temporal control of gene expression in adult tissues, the tubGal80^{ts} was employed, allowing restriction of Gal4 activity to a specific time window. Fly crosses were initially maintained at 18°C, and after adult eclosion, the progenies were transferred to 29°C, where they remained until dissection. An exception was made for the Bnl knockdown experiments shown in Figure 4, which were performed without the tubGal80^{ts} transgene.

Generation of SME-FRT-stop-FRT-Gal4 fly line and flip-out induction procedure.

SME (Shavenbaby Muscle Enhancer) is one of several enhancers of the *shavenbaby* gene (VT057071-Gal4). It is active in larval muscle progenitors (AMPs) (Figure S3 A-A') and remains active in a subpopulation of localized muscle nuclei in the adult indirect flight muscles (IFMs) (Figure S3 B-B'). To generate the SME-FRT-stop-FRT-Gal4 construct, the cis-regulatory element from the original *shavenbaby* enhancer construct was used to replace the *pAct* promoter in the pAct-FRT-stop-FRT3-FRT-FRT3-Gal4 vector (Addgene plasmid #52889). The resulting construct was integrated into the attP site at cytological location 51D on chromosome II via embryo injection into vas-int; attP-51D flies. To induce localized overexpression of Bnl::GFP in adult IFM nuclei, hsflp; FRT-SME-stop-FRT-Gal4/CyO; tubGal80^{ts} females were crossed to UAS-Bnl::GFP males. Progeny were raised at 18°C and subjected to a 2-hour heat shock at 37°C in young adulthood (Figure 4 A-C').

Immunohistochemistry and confocal microscopy

Preparation and immunofluorescence of wing discs and adult muscles were performed as previously described in (Leroux et al., 2023). The following primary antibody were used: Chicken anti-βGal (1:100, Abcam, ab9361), Chicken anti-GFP (1:300, Abcam, ab13970), Mouse anti-Mhc (1:200, DSHB, 3E8-3D3-s) , Mouse anti-dSRF (1:20, a gift from Mark A. Krasnow, Stanford university California , USA), Rabbit anti-Mef2 (1:500 , DSHB, Mef2-p), Rabbit anti-PH3 (1:100, Cell Signaling Technology, #9713), Rabbit anti-SPARC (1:500, a gift from Maurice Ringuette, University of Toronto, Canada), Rat anti-RFP (1:800, Chromotek, 5F8-20), Rabbit anti-Zfh1 (1:5000, a gift from Ruth Lehmann, New York, USA), Alexa-conjugated Phalloidin (1:200, Thermo fisher scientific life technologies).

Induction of flight muscle injury

Flight muscle injury was induced following previously described protocols (Chakraborty et al., 2018). Young adult flies (2-3 days post-eclosion) were anesthetized and positioned laterally under a stereomicroscope. A single, localized stab wound was

inflicted manually using a fine stainless-steel needle (Minutien Pins, 0.1 mm diameter; #26002–10) to minimize tissue damage and avoid extensive injury. Age-matched, uninjured flies served as controls.

Microscopy and data analysis

Samples were imaged using a Leica SP8 microscope (BIOSIT, University of Rennes) at 20×, 40×, or 63× magnification and a resolution of 1024×1024 pixels. Images were processed with ImageJ and assembled using Adobe Illustrator. To quantify fluorescence intensity, all samples were processed and analyzed in parallel under identical conditions. Confocal images were acquired using the same laser settings across all samples. Sum slice projections were generated from each confocal stack. Regions of interest (ROIs) were manually defined based on protein expression, and mean fluorescence intensities were measured within each ROI. These values were then normalized to background levels measured in comparable areas of the same sample.

Tracheal branches were visualized either by their intrinsic autofluorescence using a 405 nm UV laser (Sauerwald et al., 2019) or by the expression of membrane-bound GFP driven by a tracheal-specific Gal4 driver (UAS-mCD8GFP). Tracheal coverage was quantified as pixel area per muscle fiber from maximum intensity Z-projections acquired at 20× magnification. Quantification was performed using the “Skeletonize” plugin in ImageJ, based on the method described by Perochon et al. (2021), with minor modifications. Briefly, maximum intensity projections were generated from each confocal stack, tracheal branches were segmented by thresholding, and the resulting images were skeletonized. Skeleton pixel intensity was then measured specifically within injured muscle fibers and their corresponding contralateral control fibers. For Figure 2E, square regions of interest (ROIs) were placed at the injury site, as well as in proximal and distal regions, to assess local tracheal enrichment. Hemocyte and dSRF-positive cell numbers were quantified manually using ImageJ.

Graphs and statistical analyses were performed using GraphPad Prism. Pair comparisons were statistically tested with a two-sided Student’s t-test. NS, not significant ($p>0.05$); *$p < 0.05$, **$p < 0.01$, ***$p < 0.001$ ****$p< 0.0001$.

Acknowledgments

We would like to thank Jennifer Zanet, Cedric Polesello, Sougata Roy, Ruth Lehmann, Maurice Ringuette, Jean-Paul Vincent, and Mark A. Krasnow, as well as the Bloomington Drosophila Stock Center, the Vienna Drosophila Resource Center (VDRC), and the Developmental Studies Hybridoma Bank for providing *Drosophila* strains and antibodies. We are grateful to Lucas Waltzer, Laetitia Bataille, Alain Vincent, and Michèle Crozatier for their critical reading of the manuscript, and to other members of H.B's laboratory for valuable discussions. We also thank Emmanuel Gallaud for helpful input during the early phases of the project. We acknowledge Xavier Pinson from the Microscopy Rennes Imaging Center (MRic, BIOSIT, Biogenouest) for technical assistance, and Cyrille Surbled for fly stock maintenance and technical help. Work in the Boukhatmi lab was supported by an AFM-Téléthon Trampoline Grant (#23108), ATIP-Avenir (CNRS), and ANR GenepiMuSC (ANR-23-CE13-0006). N.A. was supported by an AFM-Téléthon PhD fellowship (#23846) and an FRM fellowship (FDT202404018608). Work in the Cordero lab was supported by a Sir Henry Dale Fellowship (Wellcome Trust and Royal Society, 104103/Z/14/Z), a Wellcome ISSF Returner Scheme (204820/Z/16/Z), and a Tenovus Fellowship (Tenovus/S22-28) to J.P.

Competing interest

The authors declare that they have no competing interests.

Reference

Antonello, Z.A., Reiff, T., Ballesta-Illan, E., Dominguez, M., 2015. Robust intestinal homeostasis relies on cellular plasticity in enteroblasts mediated by miR-8-Escargot switch. EMBO J 34, 2025-2041.

Baghdadi, M.B., Castel, D., Machado, L., Fukada, S.I., Birk, D.E., Relaix, F., Tajbakhsh, S., Mourikis, P., 2018. Reciprocal signalling by Notch-Collagen V-CALCR retains muscle stem cells in their niche. Nature 557, 714-718.

Borchiellini, C., Coulon, J., Le Parco, Y., 1996. The function of type IV collagen during Drosophila muscle development. Mech Dev 58, 179-191.

Boukhatmi, H., 2021. Drosophila, an Integrative Model to Study the Features of Muscle Stem Cells in Development and Regeneration. Cells 10.

Boukhatmi, H., Bray, S., 2018. A population of adult satellite-like cells in Drosophila is maintained through a switch in RNA-isoforms. Elife 7.

Boulet, M., Renaud, Y., Lapraz, F., Benmimoun, B., Vandel, L., Waltzer, L., 2021. Characterization of the Drosophila Adult Hematopoietic System Reveals a Rare Cell Population With Differentiation and Proliferation Potential. Front Cell Dev Biol 9, 739357.

Bradshaw, A.D., 2009. The role of SPARC in extracellular matrix assembly. J Cell Commun Signal 3, 239-246.

Bunt, S., Hooley, C., Hu, N., Scahill, C., Weavers, H., Skaer, H., 2010. Hemocyte-secreted type IV collagen enhances BMP signaling to guide renal tubule morphogenesis in Drosophila. Dev Cell 19, 296-306.

Catalani, E., Zecchini, S., Giovarelli, M., Cherubini, A., Del Quondam, S., Brunetti, K., Silvestri, F., Roux-Biejat, P., Napoli, A., Casati, S.R., Ceci, M., Romano, N., Bongiorni, S., Prantera, G., Clementi, E., Perrotta, C., De Palma, C., Cervia, D., 2022. RACK1 is evolutionary conserved in satellite stem cell activation and adult skeletal muscle regeneration. Cell Death Discovery 8, 459.

Chakraborty, K., VijayRaghavan, K., Gunage, R., 2018. A Method to Injure, Dissect and Image Indirect Flight Muscle of Drosophila. Bio Protoc 8, e2860.

Chaturvedi, D., Reichert, H., Gunage, R.D., VijayRaghavan, K., 2017. Identification and functional characterization of muscle satellite cells in Drosophila. Elife 6.

Chechenova, M., McLendon, L., Dallas, B., Stratton, H., Kiani, K., Gerberich, E., Alekseyenko, A., Tamba, N., An, S., Castillo, L., Czajkowski, E., Talley, C., Brown, A., Bryantsev, A.L., 2024. Muscle degeneration in aging Drosophila flies: the role of mechanical stress. Skelet Muscle 14, 20.

Chioran, A., Duncan, S., Catalano, A., Brown, T.J., Ringuette, M.J., 2017. Collagen IV trafficking: The inside-out and beyond story. Dev Biol 431, 124-133.

Chu, W.C., Hayashi, S., 2021. Mechano-chemical enforcement of tendon apical ECM into nano-filaments during Drosophila flight muscle development. Curr Biol 31, 1366-1378 e1367.

Dort, J., Fabre, P., Molina, T., Dumont, N.A., 2019. Macrophages Are Key Regulators of Stem Cells during Skeletal Muscle Regeneration and Diseases. Stem Cells Int 2019, 4761427.

Du, L., Sohr, A., Yan, G., Roy, S., 2018. Feedback regulation of cytoneme-mediated transport shapes a tissue-specific FGF morphogen gradient. Elife 7.

Ebner, A., Kiefer, F.N., Ribeiro, C., Petit, V., Nussbaumer, U., Affolter, M., 2002. Tracheal development in Drosophila melanogaster as a model system for studying the development of a branched organ. Gene 287, 55-66.

Eming, S.A., Martin, P., Tomic-Canic, M., 2014. Wound repair and regeneration: mechanisms, signaling, and translation. Sci Transl Med 6, 265sr266.
Ghabrial, A., Luschnig, S., Metzstein, M.M., Krasnow, M.A., 2003. Branching morphogenesis of the Drosophila tracheal system. Annu Rev Cell Dev Biol 19, 623-647.
Goh, K.Y., Lee, W.X., Choy, S.M., Priyadarshini, G.K., Chua, K., Tan, Q.H., Low, S.Y., Chin, H.S., Wong, C.S., Huang, S.Y., Fu, N.Y., Nishiyama, J., Harmston, N., Tang, H.W., 2024. FOXO-regulated DEAF1 controls muscle regeneration through autophagy. Autophagy 20, 2632-2654.
Gold, K.S., Bruckner, K., 2015. Macrophages and cellular immunity in Drosophila melanogaster. Semin Immunol 27, 357-368.
Gunage, R.D., Dhanyasi, N., Reichert, H., VijayRaghavan, K., 2017. Drosophila adult muscle development and regeneration. Semin Cell Dev Biol 72, 56-66.
Hayashi, S., Kondo, T., 2018. Development and Function of the Drosophila Tracheal System. Genetics 209, 367-380.
Jarecki, J., Johnson, E., Krasnow, M.A., 1999. Oxygen regulation of airway branching in Drosophila is mediated by branchless FGF. Cell 99, 211-220.
Kalra, S., Bahendeka, S., Sahay, R., Ghosh, S., Md, F., Orabi, A., Ramaiya, K., Al Shammari, S., Shrestha, D., Shaikh, K., Abhayaratna, S., Shrestha, P.K., Mahalingam, A., Askheta, M., AA, A.R., Eliana, F., Shrestha, H.K., Chaudhary, S., Ngugi, N., Mbanya, J.C., Aye, T.T., Latt, T.S., Akanov, Z.A., Syed, A.R., Tandon, N., Unnikrishnan, A.G., Madhu, S.V., Jawa, A., Chowdhury, S., Bajaj, S., Das, A.K., 2018. Consensus Recommendations on Sulfonylurea and Sulfonylurea Combinations in the Management of Type 2 Diabetes Mellitus - International Task Force. Indian J Endocrinol Metab 22, 132-157.
Kirkwood, T.B., 2005. Understanding the odd science of aging. Cell 120, 437-447.
Laurichesse, Q., Soler, C., 2020. Muscle development : a view from adult myogenesis in Drosophila. Semin Cell Dev Biol 104, 39-50.
Leroux, E., Ammar, N., Moinet, S., Pecot, T., Boukhatmi, H., 2023. Studying Muscle Transcriptional Dynamics at Single-molecule Scales in Drosophila. J Vis Exp.
Li, J., Zhang, S., Amaya, E., 2016. The cellular and molecular mechanisms of tissue repair and regeneration as revealed by studies in Xenopus. Regeneration (Oxf) 3, 198-208.
Lin, L., 2009. Clonal Analysis of Growth Behaviors During Drosophila Larval Tracheal Development In Doctoral thesis. University of Basel.
Marcetteau, J., Duarte, P., Leitao, A.B., Sucena, E., 2025. Transdifferentiation of plasmatocytes to crystal cells in the lymph gland of Drosophila melanogaster. EMBO Rep 26, 2077-2097.
Mase, A., Augsburger, J., Bruckner, K., 2021. Macrophages and Their Organ Locations Shape Each Other in Development and Homeostasis - A Drosophila Perspective. Front Cell Dev Biol 9, 630272.
Molina, T., Fabre, P., Dumont, N.A., 2021. Fibro-adipogenic progenitors in skeletal muscle homeostasis, regeneration and diseases. Open Biol 11, 210110.
Murphy, M.M., Lawson, J.A., Mathew, S.J., Hutcheson, D.A., Kardon, G., 2011. Satellite cells, connective tissue fibroblasts and their interactions are crucial for muscle regeneration. Development 138, 3625-3637.
Orfanos, Z., Sparrow, J.C., 2013. Myosin isoform switching during assembly of the Drosophila flight muscle thick filament lattice. J Cell Sci 126, 139-148.

Perochon, J., Yu, Y., Aughey, G.N., Medina, A.B., Southall, T.D., Cordero, J.B., 2021. Dynamic adult tracheal plasticity drives stem cell adaptation to changes in intestinal homeostasis in Drosophila. Nat Cell Biol 23, 485-496.
Peterson, S.J., Krasnow, M.A., 2015. Subcellular trafficking of FGF controls tracheal invasion of Drosophila flight muscle. Cell 160, 313-323.
Rao, P.R., Lin, L., Huang, H., Guha, A., Roy, S., Kornberg, T.B., 2015. Developmental compartments in the larval trachea of Drosophila. Elife 4.
Relaix, F., Bencze, M., Borok, M.J., Der Vartanian, A., Gattazzo, F., Mademtzoglou, D., Perez-Diaz, S., Prola, A., Reyes-Fernandez, P.C., Rotini, A., Taglietti, t., 2021. Perspectives on skeletal muscle stem cells. Nature Communications 12, 692.
Rodrigues, D., Renaud, Y., VijayRaghavan, K., Waltzer, L., Inamdar, M.S., 2021. Differential activation of JAK-STAT signaling reveals functional compartmentalization in Drosophila blood progenitors. Elife 10.
Sanchez Bosch, P., Makhijani, K., Herboso, L., Gold, K.S., Baginsky, R., Woodcock, K.J., Alexander, B., Kukar, K., Corcoran, S., Jacobs, T., Ouyang, D., Wong, C., Ramond, E.J.V., Rhiner, C., Moreno, E., Lemaitre, B., Geissmann, F., Bruckner, K., 2019. Adult Drosophila Lack Hematopoiesis but Rely on a Blood Cell Reservoir at the Respiratory Epithelia to Relay Infection Signals to Surrounding Tissues. Dev Cell 51, 787-803 e785.
Sarov, M., Barz, C., Jambor, H., Hein, M.Y., Schmied, C., Suchold, D., Stender, B., Janosch, S., K, J.V., Krishnan, R.T., Krishnamoorthy, A., Ferreira, I.R., Ejsmont, R.K., Finkl, K., Hasse, S., Kampfer, P., Plewka, N., Vinis, E., Schloissnig, S., Knust, E., Hartenstein, V., Mann, M., Ramaswami, M., VijayRaghavan, K., Tomancak, P., Schnorrer, F., 2016. A genome-wide resource for the analysis of protein localisation in Drosophila. Elife 5, e12068.
Sauerwald, J., Backer, W., Matzat, T., Schnorrer, F., Luschnig, S., 2019. Matrix metalloproteinase 1 modulates invasive behavior of tracheal branches during entry into Drosophila flight muscles. Elife 8.
Schuler, S.C., Liu, Y., Dumontier, S., Grandbois, M., Le Moal, E., Cornelison, D., Bentzinger, C.F., 2022. Extracellular matrix: Brick and mortar in the skeletal muscle stem cell niche. Front Cell Dev Biol 10, 1056523.
Shahab, J., Baratta, C., Scuric, B., Godt, D., Venken, K.J., Ringuette, M.J., 2015. Loss of SPARC dysregulates basal lamina assembly to disrupt larval fat body homeostasis in Drosophila melanogaster. Dev Dyn 244, 540-552.
Shin, M., Chang, E., Lee, D., Kim, N., Cho, B., Cha, N., Koranteng, F., Song, J.J., Shim, J., 2024. Drosophila immune cells transport oxygen through PPO2 protein phase transition. Nature 631, 350-359.
Siles, L., Ninfali, C., Cortes, M., Darling, D.S., Postigo, A., 2019. ZEB1 protects skeletal muscle from damage and is required for its regeneration. Nature Communications 10, 1364.
Subasi, B.S., Grabe, V., Kaltenpoth, M., Rolff, J., Armitage, S.A.O., 2024. How frequently are insects wounded in the wild? A case study using Drosophila melanogaster. R Soc Open Sci 11, 240256.
Sun, F., Poss, K.D., 2023. Inter-organ communication during tissue regeneration. Development 150.
Tamamouna, V., Rahman, M.M., Petersson, M., Charalambous, I., Kux, K., Mainor, H., Bolender, V., Isbilir, B., Edgar, B.A., Pitsouli, C., 2021. Remodelling of oxygen-transporting tracheoles drives intestinal regeneration and tumorigenesis in Drosophila. Nat Cell Biol 23, 497-510.

Varland, S., Silva, R.D., Kjosas, I., Faustino, A., Bogaert, A., Billmann, M., Boukhatmi, H., Kellen, B., Costanzo, M., Drazic, A., Osberg, C., Chan, K., Zhang, X., Tong, A.H.Y., Andreazza, S., Lee, J.J., Nedyalkova, L., Usaj, M., Whitworth, A.J., Andrews, B.J., Moffat, J., Myers, C.L., Gevaert, K., Boone, C., Martinho, R.G., Arnesen, T., 2023. N-terminal acetylation shields proteins from degradation and promotes age-dependent motility and longevity. Nat Commun 14, 6774.
Wu, W.H., Kuo, T.H., Kao, C.W., Girardot, C., Hung, S.J., Liu, T., Furlong, E.E.M., Liu, Y.H., 2019. Expanding the mesodermal transcriptional network by genome-wide identification of Zinc finger homeodomain 1 (Zfh1) targets. FEBS Lett 593, 1698-1710.
Zhao, Y., Alexandre, C., Kelly, G., Perez-Mockus, G., Vincent1, J.-P., 2024. Growth-induced physiological hypoxia correlates with growth deceleration during normal development. bioRxiv.

Figure legends

Figure 1. Hemocytes are specifically recruited to the damaged muscle fiber. (A-F). Adult indirect flight muscles (IFMs) imaged under uninjured conditions and at 2- and 5-days post-injury (2DPI and 5DPI) following localized stab injury. Mhc (magenta) marks muscles. Hemocytes (green) are visualized using the following reporters: *Pxn-RFP* in (A-C'') and *Enh3-Gal4; UAS-mCD8GFP* in (D-F''). Dashed yellow outlines indicate injured muscle fibers showing elevated Mhc expression. **(G).** Quantification of normalized Mhc intensity level in uninjured and injured fiber at 2DPI and 5DPI (dashed lines). In each condition light and dark shading indicate data points from three independent replicates (****p<0.0001, Student t-test; *n > 10* heminota per condition). **(H).** Schematic representation of the proportion of recruited hemocytes expressing different reporters. **(H').** Time-course analysis of hemocytes recruitment at 1, 2, 3, 4, and 5DPI reveals heterogeneous kinetics of response to muscle damage. Enh3-positive, Pxn-positive, and Hml-positive hemocytes are represented by light gray, black, and dark gray bars, respectively (****p < 0.0001, Student's t-test; *n ≥ 10* heminota per condition). **(I-J''').** Distribution of hemocytes visualized with *Enh3-Gal4; UAS-mCD8GFP* (green) in control muscles (I-I''') and *Naa30* mutants (J-J'''). Muscles and muscle nuclei are stained with Mhc (magenta) and Mef2 (cyan) respectively. Scale bar: 100µm. Asterisks in panels I''' and J''' mark non-specific signal detected in motoneurons.

Figure 2. Muscle damage induces directed tracheal remodeling. (A-A'). Hemocytes (green/magenta; *Enh3-Gal4, UAS-mCD8GFP; UAS-H2B-RFP*) are associated to the tracheal cells (gray, autofluorescence). Scale bars: 25 µm. **(B-C'').** Distribution of tracheal branches (gray, autofluorescence) and hemocytes (green, *Enh3-Gal4; UAS-mCD8GFP*) in control (B-B'') and at 5DPI (C-C''). Muscles are labeled with Mhc (magenta). **(B'', C'').** Boxed regions from (B and C), magnified 2X. Scale bars: 100 µm. **(D)**. Quantification of tracheal coverage in (B) and (C) (****p < 0.0001, Student's *t*-test; *n = 19* heminota per condition; light, dark, and intermediate shading indicate data points from three independent replicates). **(E).** Quantification of tracheal coverage in (C) at the injury site (orange box), adjacent to the injury site (green box, approximately 135 µm away from the injury site), and at distant regions (blue box, within 300 µm of the lesion border) (*p= 0.0142, Student's *t*-test; *n=19* heminota). **(F-**

F'). *dSRF-Gal4* marks muscle-associated terminal tracheal cells (TTCs). TTC membranes (green) and nuclei (magenta) are indicated by arrowheads and arrows, respectively (*dSRF-Gal4, UAS-mCD8GFP; UAS-H2B-RFP*). *dSRF-Gal4* is inactive in primary tracheal branches (asterisks in F'). Muscles are labeled with Mhc (blue). Scale bars: 25 µm. **(G-H''').** TTCs distribution in IFMs (green, *dSRF-Gal4, UAS-mCD8GFP*) in control (G-G''') and at 5DPI (H-H'''). Muscles are labeled with Mhc (magenta). **(G'', H'').** 4.5X magnification of boxed regions in (G') and (H'), respectively. Scale bar: 100 µm. **(G''', H''').** Orthogonal views of (G'') and (H''). Arrow in (H''') indicates TTC enrichment at the injured muscle. **(I).** Quantification of TTCs coverage from (G) and (H) (****p < 0.0001, Student's *t*-test; *n = 14* heminota per condition; light, dark, and intermediate shading represent data points from three independent replicates). **(J-J').** dSRF (green) marks TTCs nuclei associated with muscle. Scale bars: 25 µm. **(K-L''').** Distribution of TTCs nuclei (green) in IFMs under control conditions (K-K''') and at 5DPI (L-L'''). Muscles are labeled with phalloidin (blue); tracheae are visualized by autofluorescence (gray). Anti-PH3 (magenta) is used to assess cell division. **(K', L').** 2X magnification of boxed regions in (K) and (L), respectively. Scale bars: 100 µm. Arrowheads and arrows indicate dSRF expression in the muscle and TTCs nuclei, respectively. **(M).** Proportion of TTCs nuclei located within a selected muscle relative to the total number of TTCs nuclei in the imaged sample (p = 0.036, Student's *t*-test; *n = 17* heminota per condition; light, dark, and intermediate shading indicate data points from three independent replicates).

Figure 3. Local hypoxia in response to muscle damage drives tracheal branching. (A-A''). *SyHREns* reporter activity (green) is detected in a subset of TTCs marked by dSRF (magenta, arrows). Scale bars: 25 µm. **(B-D'').** Expression of the *SyHREns* reporter (green) in control IFMs (B-B''), at 5DPI (C-C'') and 20DPI (D-D''). Muscles are labeled with Mhc (magenta), and tracheal branches are visualized via autofluorescence (gray). **(B'', C'' and D'').** 2X magnification of the boxed regions in B', C' and D'. Scale bars: 100 µm. **(E).** Quantification of SyHREns positive cells (green) per injured muscle fiber (****p < 0.0001, Student's *t*-test; *n > 20* heminota per condition; light, dark and intermediate shading indicate data points from three independent replicates). **(F-H'').** *sima* (HIF-1α) downregulation in TTCs (*dSRF-Gal4; UAS-Sima^{RNAi}*) prevents tracheal recruitment at the injured fiber. **(F'', G'' and H'').** 2X

magnification of the boxed regions in E', F' and G'. Scale bars: 100 µm. **(I)**. Quantification of trachea coverage (****p < 0.0001, Student's *t*-test; *n = 13* heminota per condition). **(J-K'').** Detection of Bnl (green, Bnl:GFP^{endo}) in control IFMs (J-J'') and at 5DPI (K-K''). Muscles are labeled with Mhc (magenta), and tracheal cells are visualized via autofluorescence (gray). **(J'', K'').** 4.5X magnification of the boxed regions in J and K. Scale bars: 100 µm. **(J''', K''').** Orthogonal views of (J) and (K). Asterisk in K''' indicates Bnl:GFP^{endo} enrichment at the injured muscle. **(L).** Quantification of normalized Bnl:GFP^{endo} intensity level in uninjured and injured muscle fiber and 5DPI (***p<0.0001, Student *t*-test, *n = 15* heminota per condition from three independent replicates).

Figure 4. Hemocytes provide Bnl ligand to injured muscle to attract tracheal cells. (A-C'). Local overexpression of UAS-Bnl::GFP (green) in adult IFMs under *SME-Gal4* control results in enrichment of terminal tracheal cells (TTCs), marked by dSRF (magenta, B' and C'), and a significant increase in tracheal branching (gray, B and C), compared to untreated controls (A). Scale bars: 100 µm**. (D-D').** Bnl (green, Bnl:GFP^{endo}) is detected in indirect flight muscles (IFMs, labelled with Mhc, blue; arrowheads), tracheal branches (autofluorescence, gray; asterisks), and hemocytes (*Pxn-RFP*, magenta; arrows). Scale bars: 25 µm. **(E-E').** Expression of the *Bnl-LacZ* reporter (green) is observed in terminal tracheal cells (TTCs) marked by dSRF (magenta; asterisks), and in IFMs nuclei (arrowheads). Scale bars: 25 µm. **(F-F').** Bnl-LacZ (green) is detected in IFMs associated hemocytes labelled with *Pxn-RFP* (magenta; arrows). Scale bars: 25 µm. **(G-H'').** Bnl expression (green, Bnl:GFP^{endo}) in control IFMs (G-G'') and at 5DPI (H-H''). Muscles are labeled with Mhc (blue), tracheal cells visualized via autofluorescence (gray), and hemocytes detected with the *Pxn-RFP* reporter (magenta). Arrows in H'' indicate Bnl localization around hemocytes recruited to the injured muscle. Scale bars: 100 µm. **(I-L).** Downregulating *bnl* in the hemocytes (green, *Enh3-Gal4; UAS-mCD8GFP, UAS-Bnl^{RNAi}*) do not alter hemocytes recruitment but decreases tracheal invasion to the damaged fiber as shown in (L'- L'') and quantified in **(M).** (**** p< 0.0001, Student t-test; *n = 16* heminota from two independent replicates). Scale bars: 100 µm.

Figure 5. Breathless (Btl) is expressed along tracheal branches and is required for tracheal recruitment to the damaged muscle. (A-B''). Btl:cherry^{endo} (magenta) is detected along tracheal branches (gray) associated with indirect flight muscles (IFMs) labelled with Mhc (cyan), in either control A' or injured muscles B'. **(A'', B'').** Boxed regions from (A-B), magnified 4.5X. Scale bars: 100 µm. **(C-C').** The *Btl-Gal4* driver (green and magenta; *Btl-Gal4, UAS-mCD8GFP; UAS-H2B-RFP*) is active in a subset of tracheal branches (arrows, C-C'). Arrowheads in C indicate the tracheal branches that do not express the *Btl-Gal4* driver. Scale bars: 25 µm. **(D-E).** Expression of the Btl-Gal4 driver (green, *Btl-Gal4, UAS-mCD8GFP*) in control (D) and at 5DPI (E). Muscles are labelled with Mhc (magenta). Scale bars: 100 µm. **(F-I'').** Downregulating *btl* in the tracheal cells with either *dSRF-Gal4* driver (*dSRF-Gal4; UAS-Btl^{RNAi},* H-H'') or Btl-Gal4 driver (*Btl-Gal4, UAS- Btl^{RNAi}*, I-I'') prevents tracheal invasion to the damaged fiber. **(J).** Quantification of trachea coverage (****$p < 0.0001$, **$p=0.0053$, Student's *t*-test; $n = 7$ heminota per condition). Scale bars: 100 µm.

Figure 6. Hemocytes derived extracellular matrix components are required for muscle maintenance. (A-A''). Vkg::GFP (green) is distributed at basal levels around muscle fibers (arrow, A'), tracheal branches (arrowheads, A'), and hemocytes (magenta, *Pxn-RFP*; arrow, A'') in control conditions. **(B-B'').** At 5DPI, Vkg::GFP is strongly enriched on the injured muscle fibers (labelled with Mhc, blue). **(C-H).** Hemocytes recruitment (magenta, *Pxn-RFP*) and Collagen IV (green, *Vkg::GFP*) distribution on the injured muscle, from 1DPI to 20DPI. Scale bars: 100 µm. **(I-J).** SPARC (magenta) is detected in the IFMs associated hemocytes visualized by either *HmlΔ-Gal4* (I-I') or *Enh3-Gal4* (J-J') drivers. **(K-K').** SPARC expression is increased in injured fibers compared to controls (J-J'). **(L-L').** Adult hemocytes (magenta; *SPARC-Gal4*, *UAS-myr-RFP*) express BM40-SPARC-GFP (green). **(M-M').** BM40-SPARC-GFP produced by adult hemocytes is broadly distributed along the injured muscle fibers. **(N-N').** Detection of adult hemocytes expressing *Enh3-Gal4, UAS-mCD8GFP; UAS-H2B-RFP* (green and magenta, arrowheads) at the distal ends of IFMs and in close proximity to the tendons (arrow). TOPRO (blue) labels muscle nuclei. Scale bars: 100 µm. **(O-P').** Downregulation of *Sparc* in adult hemocytes *(using Enh3-Gal4 driver)* induces localized muscle defects at muscle fiber tips, accompanied by upregulation of Mhc **(Q)**.

Figure 7. Coordinated hemocyte–tracheal communication drives the sequential response to muscle injury. A. *Drosophila* IFMs damage induces an upregulation of Mhc expression and is associated with local hypoxia. **B.** In response to this injury, hemocytes are specifically recruited to the damaged muscle fiber, where they: **C.** secrete Branchless (Bnl), which accumulates within the injured fiber to promote tracheal outgrowth via the Bnl/Breathless (Btl) signaling pathway, and **D.** produce extracellular matrix (ECM) components, such as Sparc and Collagen IV, which are essential for maintaining adult muscle integrity.

Extended figure legends.

Figure S1. Mhc upregulation marks the damaged muscle fiber. (A-B''). Wild-type IFMs stained for Mhc (magenta) and Mef2 (cyan) show upregulation of Mhc and downregulation of Mef2 in the injured fiber (Dashed outlines, B'-B'') at 5DPI. **(A', B').** 2X magnification of the boxed regions in A and B. Scale bars: 100 µm. **(C-C'').** Expression of the embryonic Mhc isoform (*weeP26*, green) in uninjured (C) and injured (C'-C'') IFMs. Injury does not alter weeP26 expression (C and C''). **(D-D'').** The shorter Mhc-GFP isoforms (*Mhc-Iso-K, L, M (fTRG500*); green) colocalize with anti-Mhc staining (magenta) and are upregulated in injured muscle (D-D''). **(E-E'').** The longer Mhc-GFP isoforms (*Mhc-Iso-A, F, G (fTRG519*); green) are not expressed in adult IFMs and do not respond to muscle injury (E-E''). Scale bars: 100 µm. **(F-G'').** In *Naa30* mutant IFMs, defective muscle attachment correlates with increased Mhc expression (magenta, G), upregulation of short Mhc-GFP isoforms (green, G'), and a loss of Mef2 (cyan, G''). **(H-I').** Co-expression of hemocytes markers *HmlΔ-Gal4, UAS-mCD8GFP* (green) and *Pxn-RFP* (magenta) reveals two subsets of hemocytes: $Pxn^{+}Hml^{+}$ (arrows) and $Pxn^{+}Hml^{-}$ (arrowheads). Nuclei are visualized with TO-PRO (blue). Data from *n >10* heminota from two independent replicates. **(J-M').** Co-expression analysis of *Enh3-Gal4; UAS-mcD8GFP* (green) and *Pxn-RFP* (magenta) shows that all $Enh3^{+}$ cells express Pxn (J'-K'). No Mef2 expression (cyan) is observed in these cells, in either undamaged (L') or damaged (M', dashed lines) fibers. Scale bars: 100 µm. Yellow asterisks in panels B'', F'', G'', L' and M' mark non-specific signal detected in motoneurons.

Figure S2. Early recruitment of hemocytes initiates tracheal remodeling after muscle damage. (A-B'). Hemocytes are visualized using an anti-Zfh1 (green) are

recruited to the injured fiber exhibiting elevated Mhc expression (magenta). **(C-D').** In *Naa30* mutant flies, defective muscle attachment is associated with tracheal enrichment (gray, D') and increased hemocytes accumulation (green, D') compared to controls (C-C'). **(E-M').** Time-course analysis of tracheal remodeling and hemocytes recruitment in *Enh3-Gal4; UAS-mCD8GFP* adult IFMs following localized stab injury. Tracheal branches are visualized by autofluorescence (gray), and hemocytes are labeled with GFP (green). Muscles are labeled with Mhc (magenta). Time points range from 1-hour post-injury (1HPI) to 20 days post-injury (20DPI). **(N)**. Quantification of normalized Mhc intensity. **(O)**. Quantification of the hemocytes number in the injured fiber shows a significant increase starting at 1HPI which remains elevated until 20DPI. **(P).** Tracheal quantification shows a marked increase in its density from 3DPI and remains sustained until 20 DPI. (****$p < 0.0001$, ***$p < 0.001$; Student's t-test; $n \geq 10$ heminota per condition). Scale bars: 100 µm.

Figure S3. Tracheal branching in response to muscle damage requires precise control of Bnl. (A-B'). Expression pattern of the *Shavenbaby* (*Svb*) muscle regulatory enhancer (*SME-Gal4; UAS-mCD8GFP*). *SME-Gal4* drives GFP expression (green) in a subset of larval muscle progenitors located in the posterior region of the wing disc (A-A') and in a subset of adult muscle nuclei (DAPI, blue, B-B') Scale bars: 100 µm. **(C).** Schematic representation of the *Drosophila* FLP-OUT system used for localized overexpression of UAS-Bnl::GFP in muscle nuclei, employing the *Hsflp; FRT-SME-Stop-FRT-Gal4/CyO; tub-Gal80ts* trasgenes. **(D-E").** Loss of Bnl-LacZ reporter expression (green) is specifically observed in the nuclei of the injured muscle fibers overexpressing Mhc (magenta). **(D', E').** 6X magnification of the boxed regions in D and E, Scale bars: 25 µm. **(F-H).** Targeted downregulation of *bnl* in a subset of hemocytes using *HmlΔ-Gal4* driver significantly reduces tracheal enrichment at the injured fiber, as quantified in **(I)**. (*$p < 0.05$, Student's t-test; $n \geq 10$ heminota per condition). Scale bars: 100 µm.

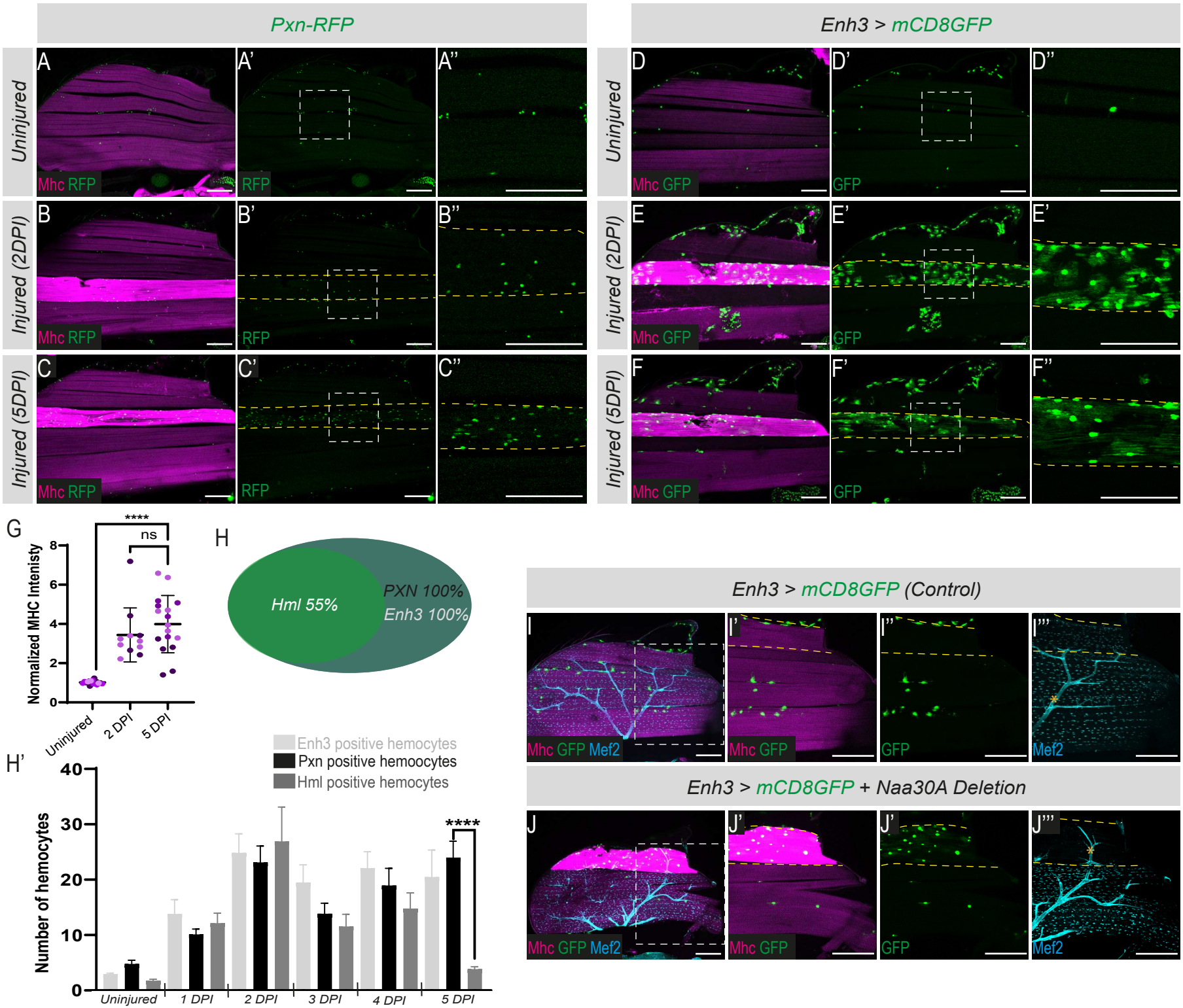
Pxn-RFP
Enh3 > mCD8GFP
Uninjured
Injured (2DPI)
Injured (5DPI)
A
A'
A''
B
B'
B''
C
C'
C''
D
D'
D''
E
E'
E'
F
F'
F''
Mhc RFP
RFP
Mhc GFP
GFP
G
****
ns
Normalized MHC Intenisty
Uninjured
2 DPI
5 DPI
H
Hml 55%
PXN 100%
Enh3 100%
H'
Enh3 positive hemocytes
Pxn positive hemoocytes
Hml positive hemocytes
Number of hemocytes
Uninjured
1 DPI
2 DPI
3 DPI
4 DPI
5 DPI
Enh3 > mCD8GFP (Control)
I
I'
I''
I'''
Mhc GFP Mef2
Mhc GFP
GFP
Mef2
Enh3 > mCD8GFP + Naa30A Deletion
J
J'
J'
J'''

Figure 1

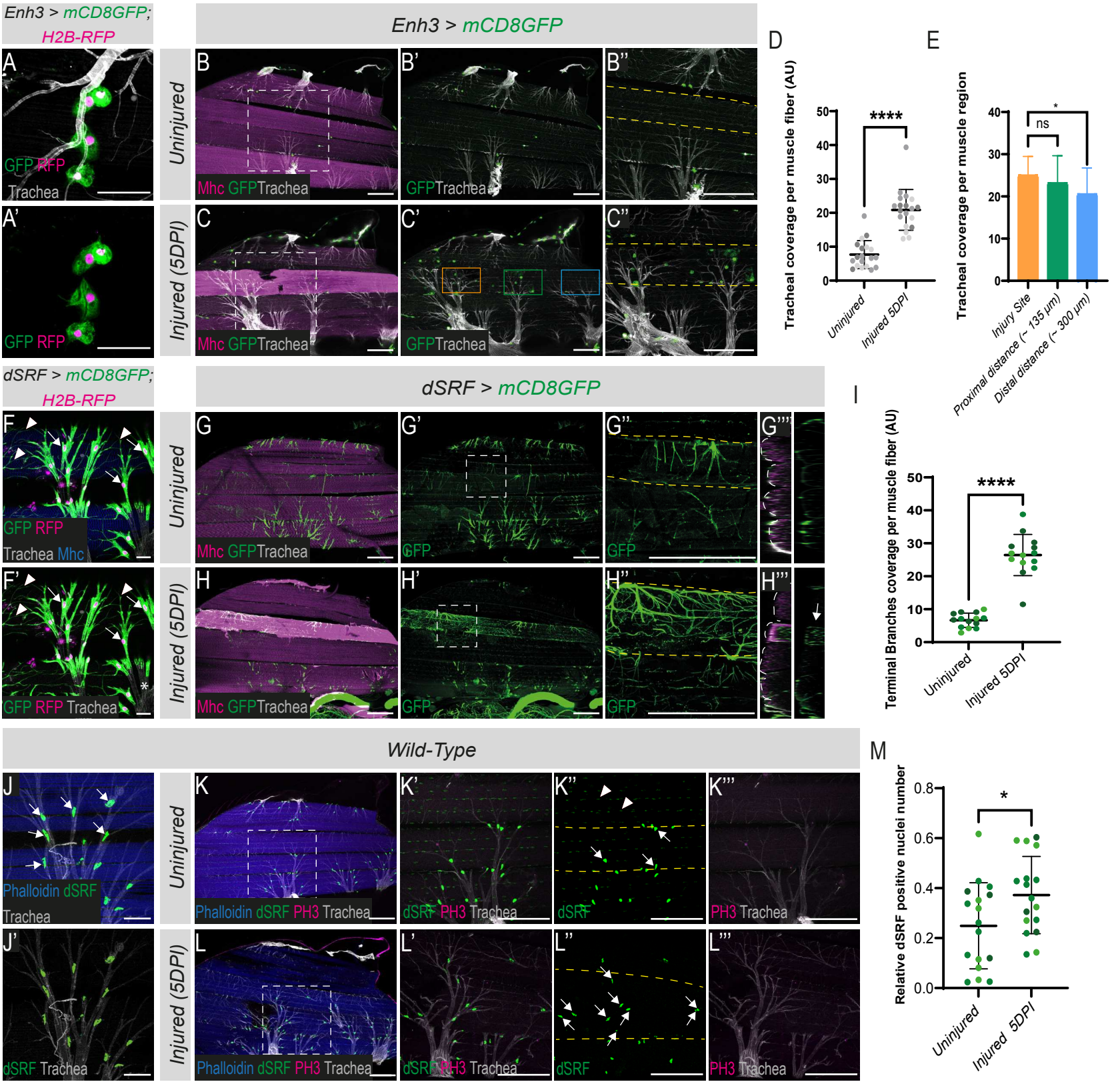
Enh3 > mCD8GFP; H2B-RFP
Enh3 > mCD8GFP
Uninjured
Injured (5DPI)
GFP RFP
Trachea
Mhc GFP Trachea
GFP Trachea
D
E
Tracheal coverage per muscle fiber (AU)
****
Uninjured
Injured 5DPI
Tracheal coverage per muscle region
ns
*
Injury Site
Proximal distance (~ 135 µm)
Distal distance (~ 300 µm)
dSRF > mCD8GFP; H2B-RFP
dSRF > mCD8GFP
GFP RFP Trachea Mhc
GFP
I
Terminal Branches coverage per muscle fiber (AU)
Wild-Type
Phalloidin dSRF Trachea
Phalloidin dSRF PH3 Trachea
dSRF PH3 Trachea
dSRF
PH3 Trachea
M
Relative dSRF positive nuclei number

Figure 2

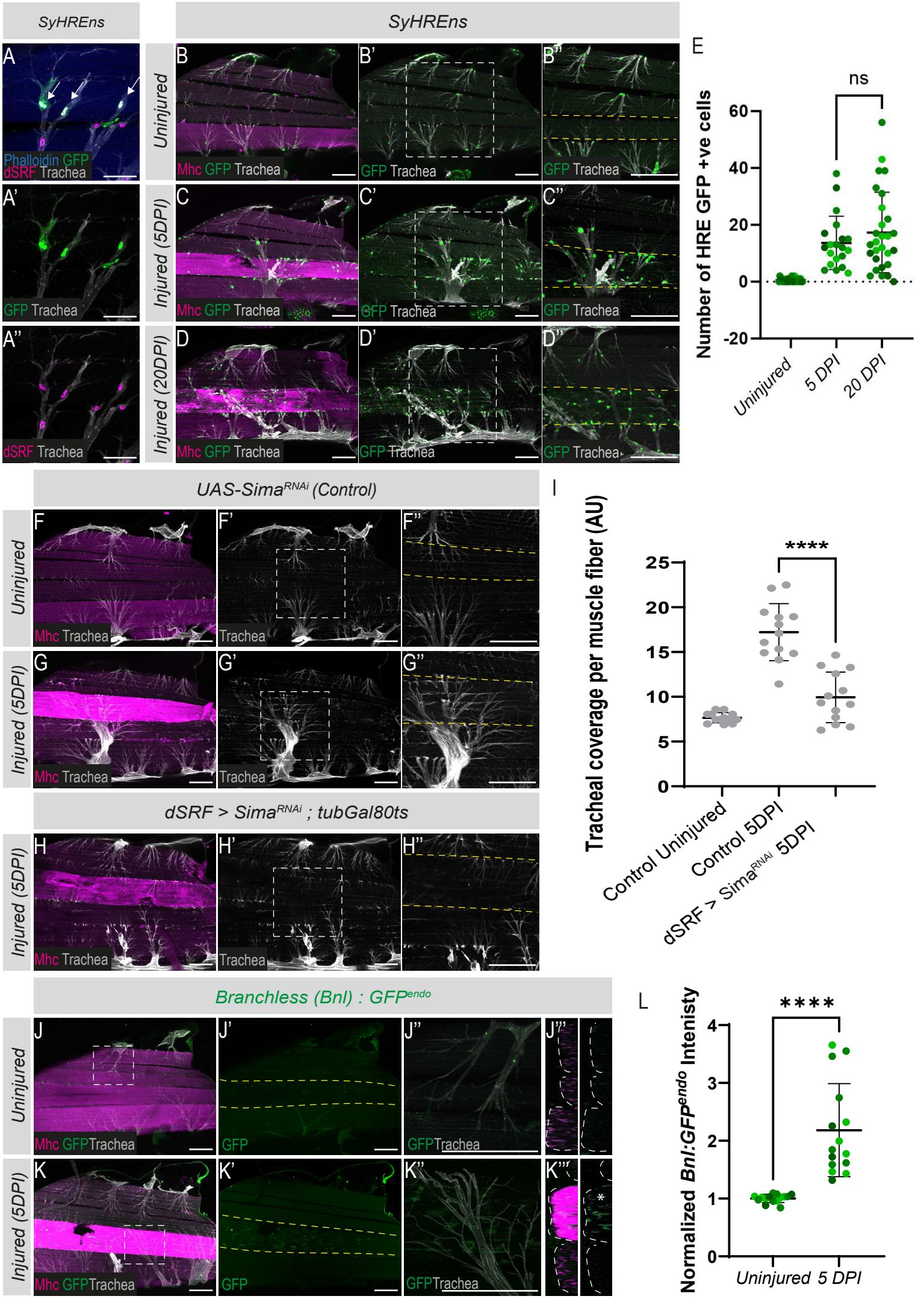
SyHREns
SyHREns
A
Phalloidin GFP
dSRF Trachea
A'
GFP Trachea
A''
dSRF Trachea
Uninjured
Injured (5DPI)
Injured (20DPI)
B
B'
B''
Mhc GFP Trachea
GFP Trachea
C
C'
C''
D
D'
D''
E
ns
Number of HRE GFP +ve cells
60
40
20
0
-20
Uninjured
5 DPI
20 DPI
UAS-Sima^RNAi (Control)
F
F'
F''
Mhc Trachea
Trachea
G
G'
G''
dSRF > Sima^RNAi ; tubGal80ts
H
H'
H''
I
****
Tracheal coverage per muscle fiber (AU)
25
20
15
10
5
0
Control Uninjured
Control 5DPI
dSRF > Sima^RNAi 5DPI
Branchless (Bnl) : GFP^endo
J
J'
J''
J'''
Mhc GFPTrachea
GFP
GFPTrachea
K
K'
K''
K'''
L
****
Normalized Bnl:GFP^endo Intenisty
4
3
2
1
0
Uninjured
5 DPI

Figure 3

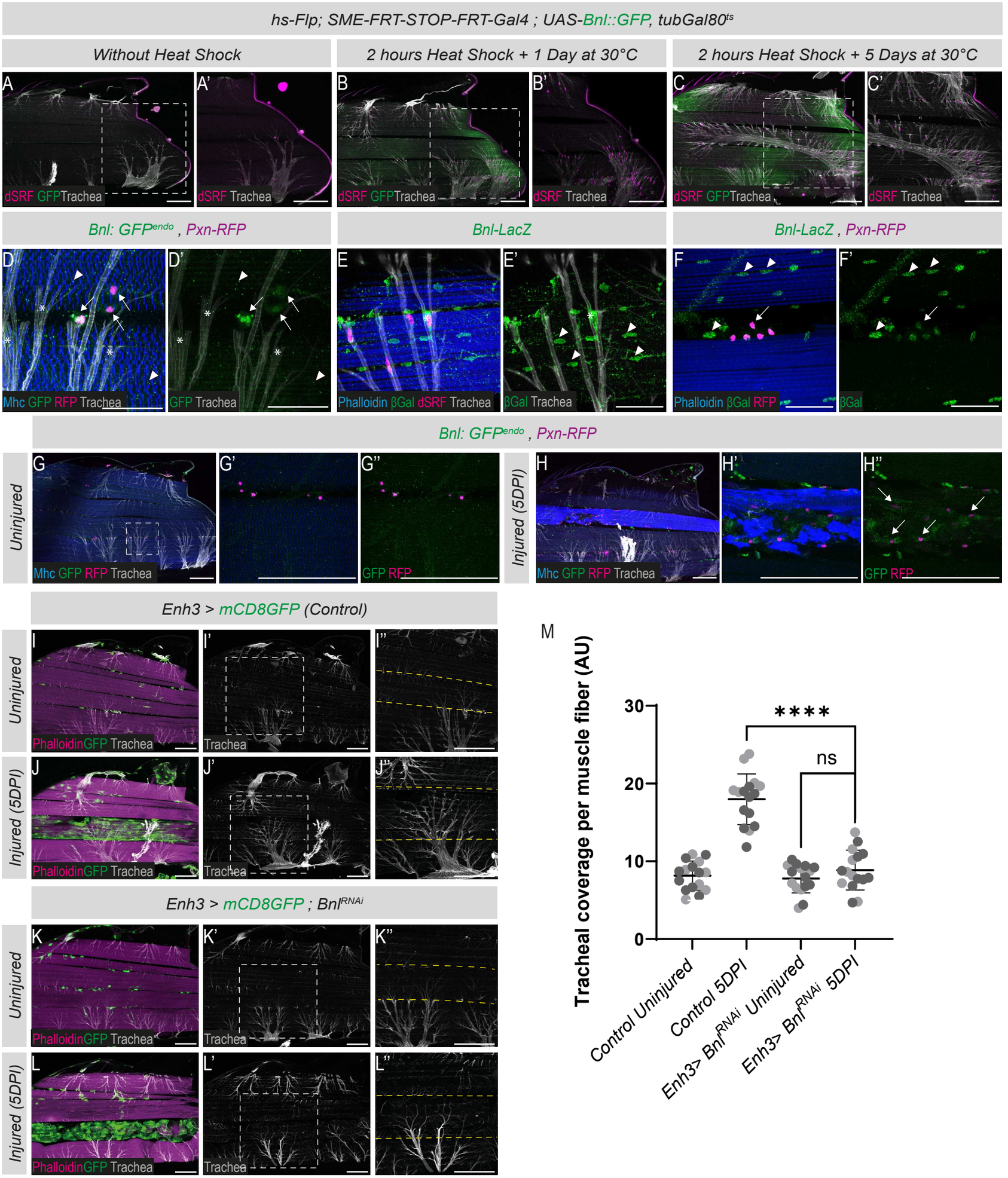
hs-Flp; SME-FRT-STOP-FRT-Gal4 ; UAS-Bnl::GFP, tubGal80ts
Without Heat Shock
2 hours Heat Shock + 1 Day at 30°C
2 hours Heat Shock + 5 Days at 30°C
A
A'
B
B'
C
C'
dSRF GFP Trachea
dSRF Trachea
Bnl: GFPendo , Pxn-RFP
Bnl-LacZ
Bnl-LacZ , Pxn-RFP
D
D'
E
E'
F
F'
Mhc GFP RFP Trachea
GFP Trachea
Phalloidin βGal dSRF Trachea
βGal Trachea
Phalloidin βGal RFP
βGal
Bnl: GFPendo , Pxn-RFP
Uninjured
Injured (5DPI)
G
G'
G''
H
H'
H''
Mhc GFP RFP Trachea
GFP RFP
Enh3 > mCD8GFP (Control)
I
I'
I''
J
J'
J''
PhalloidinGFP Trachea
Trachea
Enh3 > mCD8GFP ; BnlRNAi
K
K'
K''
L
L'
L''
M
Tracheal coverage per muscle fiber (AU)
30
20
10
0
****
ns
Control Uninjured
Control 5DPI
Enh3> BnlRNAi Uninjured
Enh3> BnlRNAi 5DPI

Figure 4

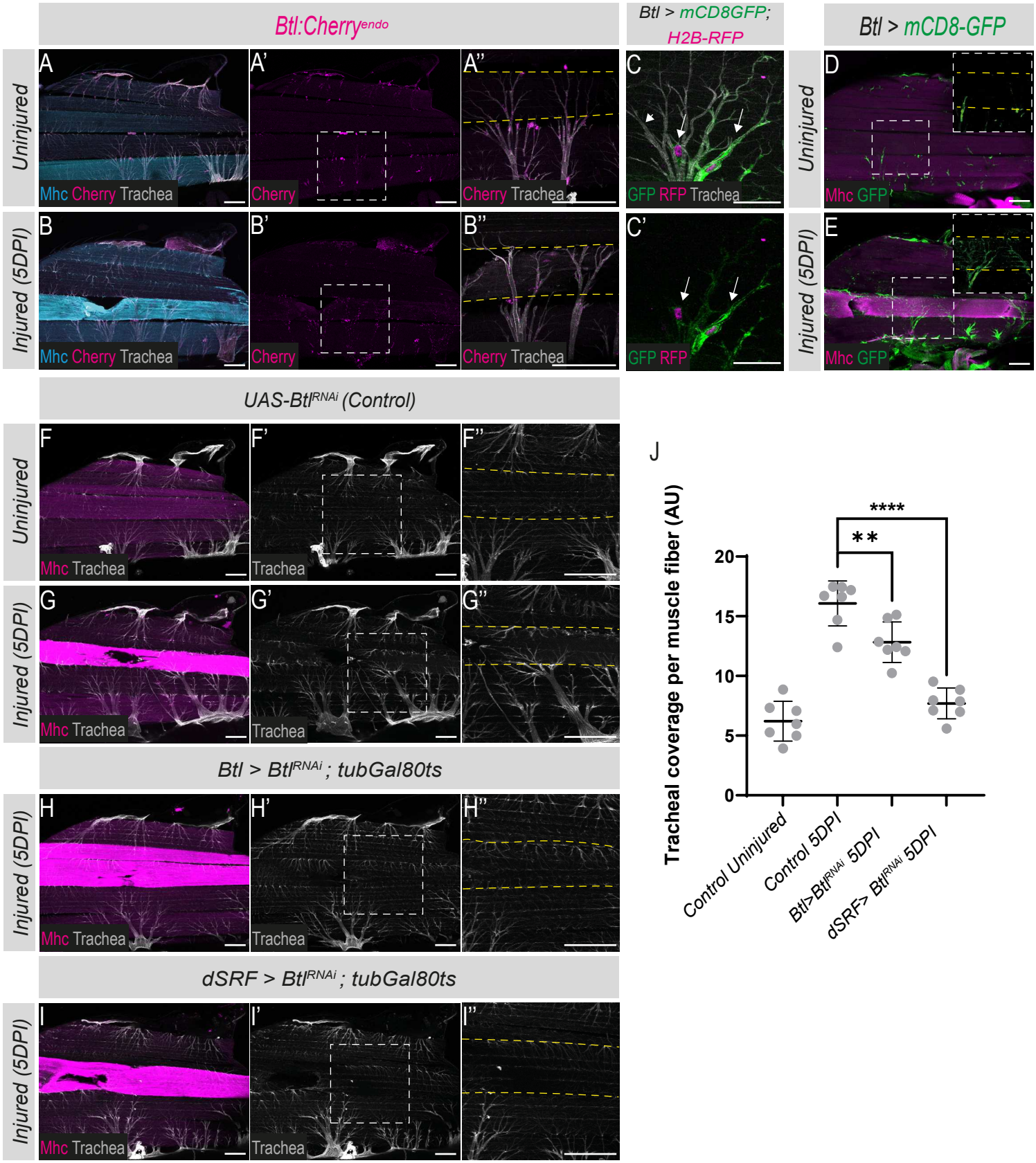
Btl:Cherryendo
Btl > mCD8GFP; H2B-RFP
Btl > mCD8-GFP
Uninjured
Injured (5DPI)
A
A'
A''
B
B'
B''
C
C'
D
E
Mhc Cherry Trachea
Cherry
Cherry Trachea
GFP RFP Trachea
GFP RFP
Mhc GFP
UAS-BtlRNAi (Control)
F
F'
F''
G
G'
G''
Mhc Trachea
Trachea
Btl > BtlRNAi ; tubGal80ts
H
H'
H''
dSRF > BtlRNAi ; tubGal80ts
I
I'
I''
J
Tracheal coverage per muscle fiber (AU)
0
5
10
15
20
**
****
Control Uninjured
Control 5DPI
Btl>BtlRNAi 5DPI
dSRF> BtlRNAi 5DPI

Figure 5

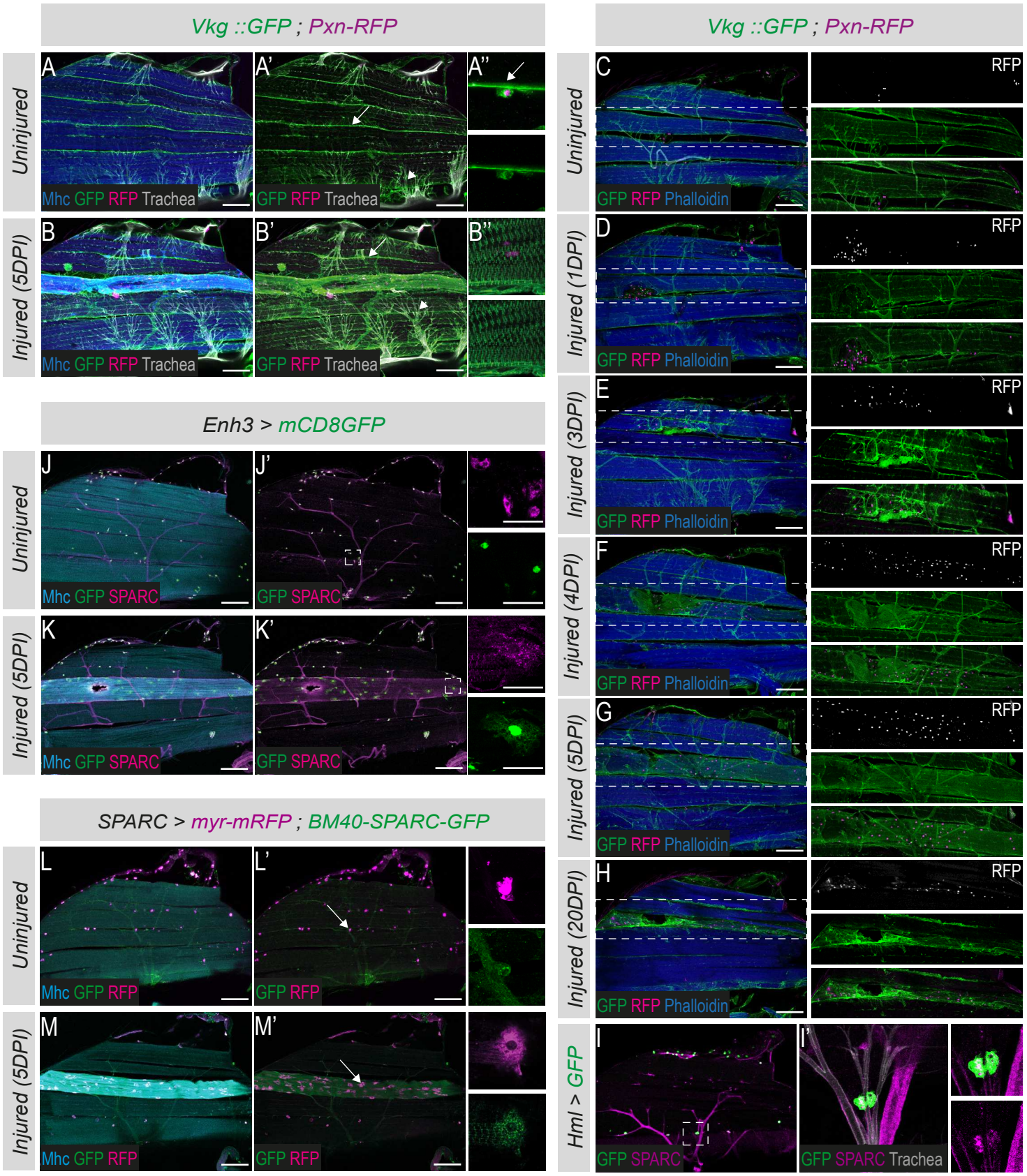
Vkg ::GFP ; Pxn-RFP
Uninjured
Injured (5DPI)
A
A'
A''
B
B'
B''
Mhc GFP RFP Trachea
GFP RFP Trachea
Enh3 > mCD8GFP
J
J'
K
K'
Mhc GFP SPARC
GFP SPARC
SPARC > myr-mRFP ; BM40-SPARC-GFP
L
L'
M
M'
Mhc GFP RFP
GFP RFP
Vkg ::GFP ; Pxn-RFP
Injured (1DPI)
Injured (3DPI)
Injured (4DPI)
Injured (5DPI)
Injured (20DPI)
C
D
E
F
G
H
RFP
GFP RFP Phalloidin
Hml > GFP
I
I'
GFP SPARC
GFP SPARC Trachea

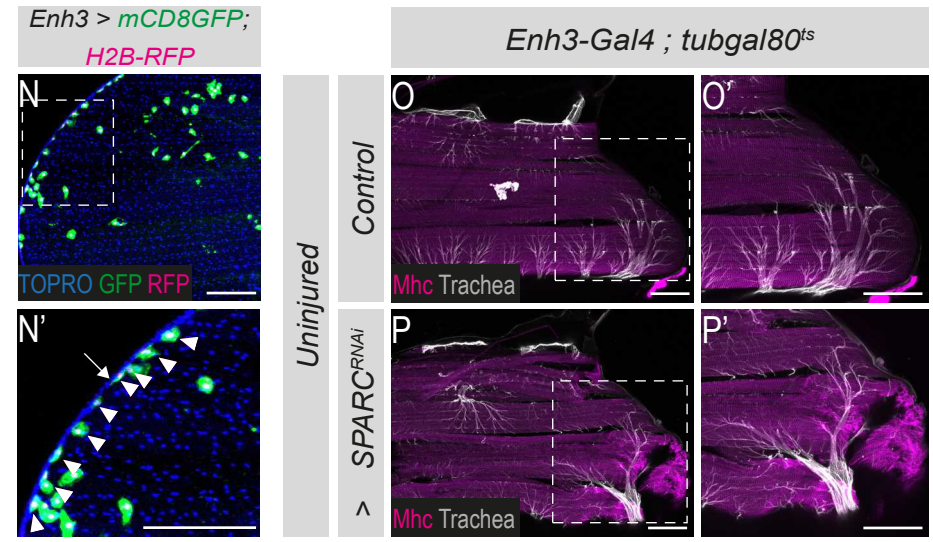
Enh3 > mCD8GFP;
H2B-RFP
N
N'
TOPRO GFP RFP
Enh3-Gal4 ; tubgal80ts
Uninjured
Control
> SPARCRNAi
O
O'
P
P'
Mhc Trachea

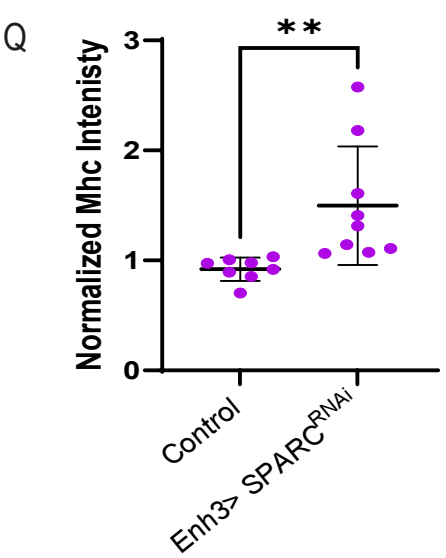
Q
Normalized Mhc Intenisty
0
1
2
3
**
Control
Enh3> SPARCRNAi

Figure 6

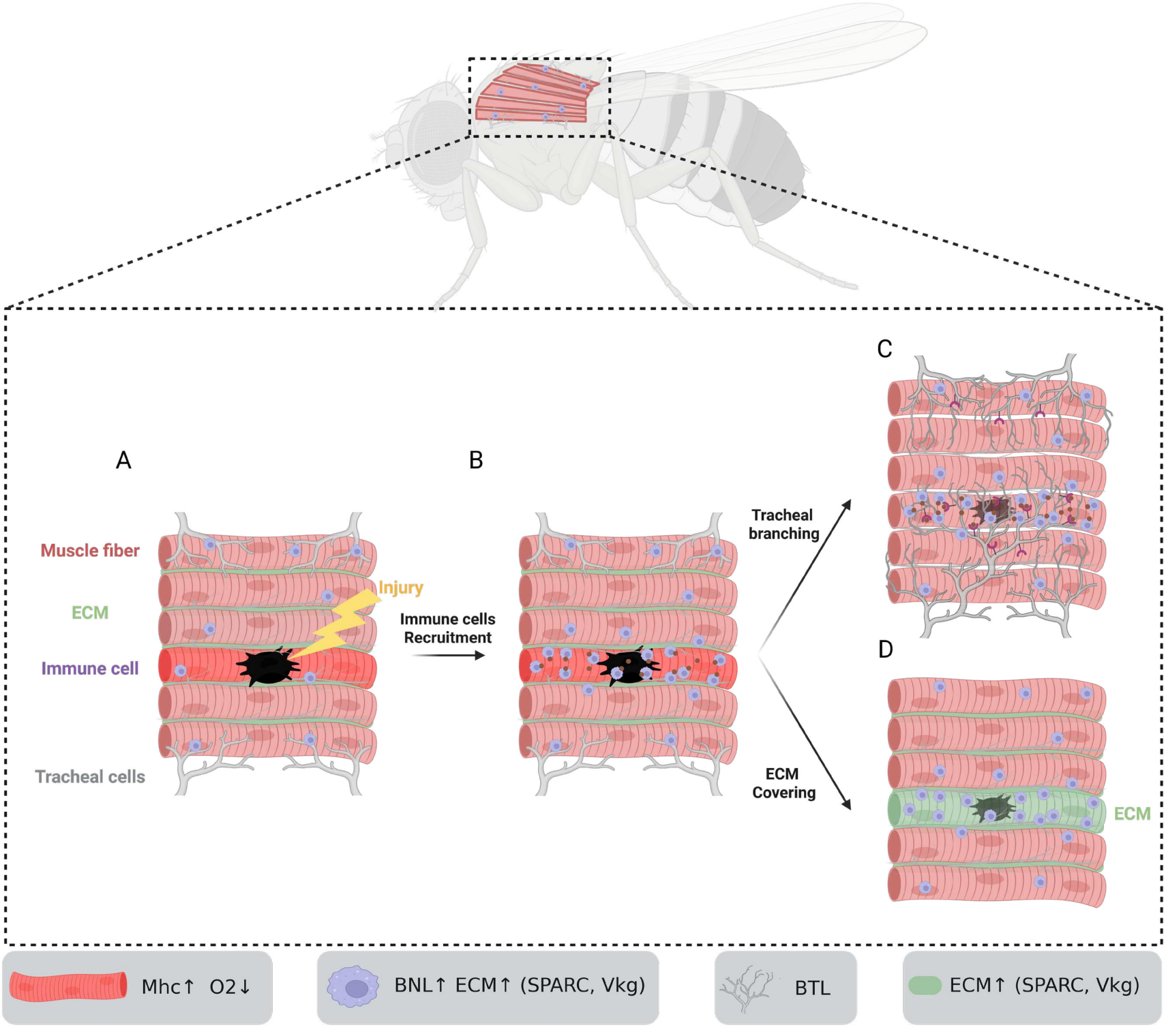
A
B
C
D
Muscle fiber
ECM
Immune cell
Tracheal cells
Injury
Immune cells
Recruitment
Tracheal
branching
ECM
Covering
ECM
Mhc↑ O2↓
BNL↑ ECM↑ (SPARC, Vkg)
BTL
ECM↑ (SPARC, Vkg)

Figure 7

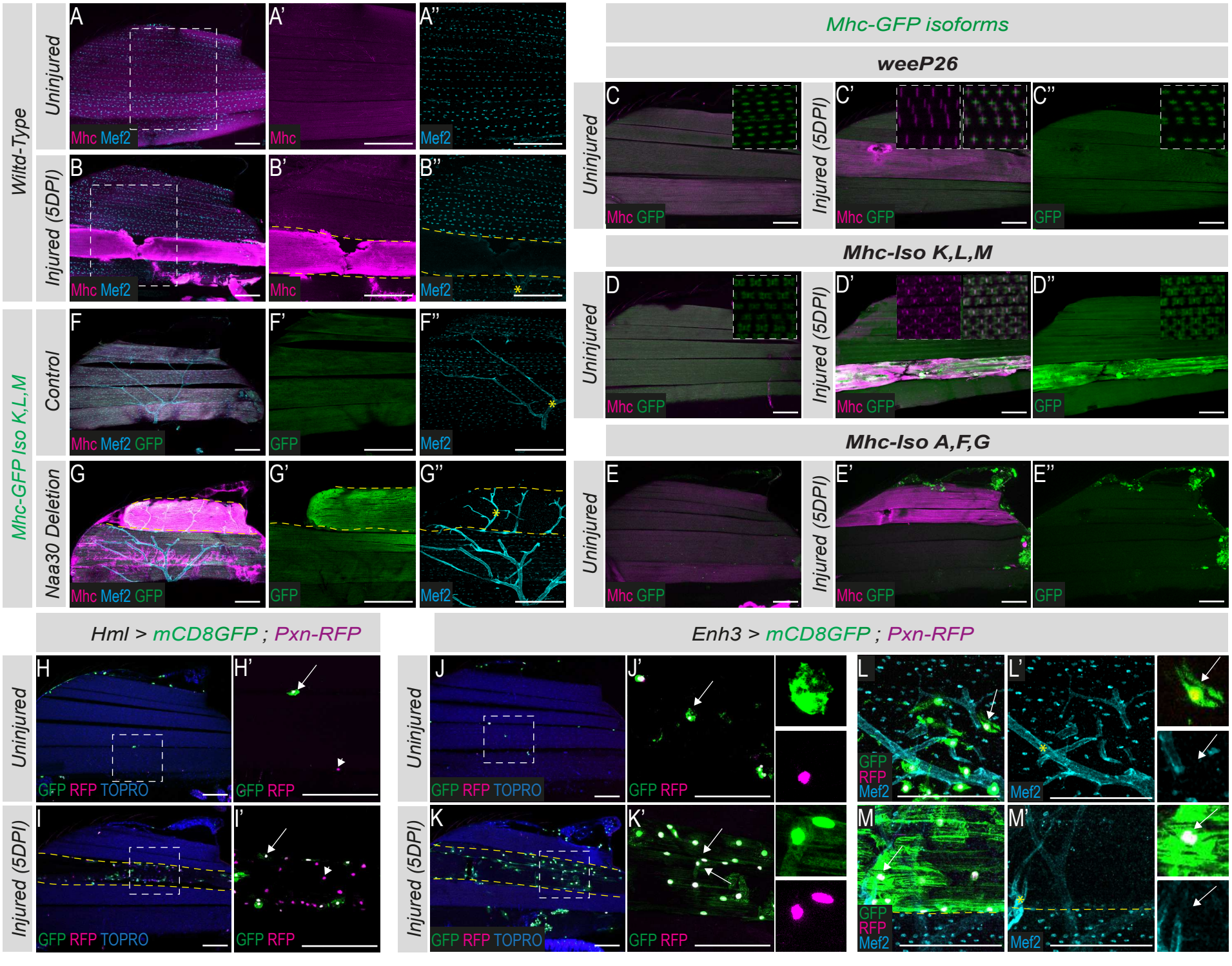
Wild-Type
Uninjured
Injured (5DPI)
Mhc-GFP Iso K,L,M
Control
Naa30 Deletion
A
A'
A''
B
B'
B''
F
F'
F''
G
G'
G''
Mhc Mef2
Mhc
Mef2
Mhc Mef2 GFP
GFP
Mhc-GFP isoforms
weeP26
Mhc-Iso K,L,M
Mhc-Iso A,F,G
C
C'
C''
D
D'
D''
E
E'
E''
Mhc GFP
Hml > mCD8GFP ; Pxn-RFP
Enh3 > mCD8GFP ; Pxn-RFP
H
H'
I
I'
J
J'
K
K'
L
L'
M
M'
GFP RFP TOPRO
GFP RFP
GFP
RFP
Mef2

Figure S1

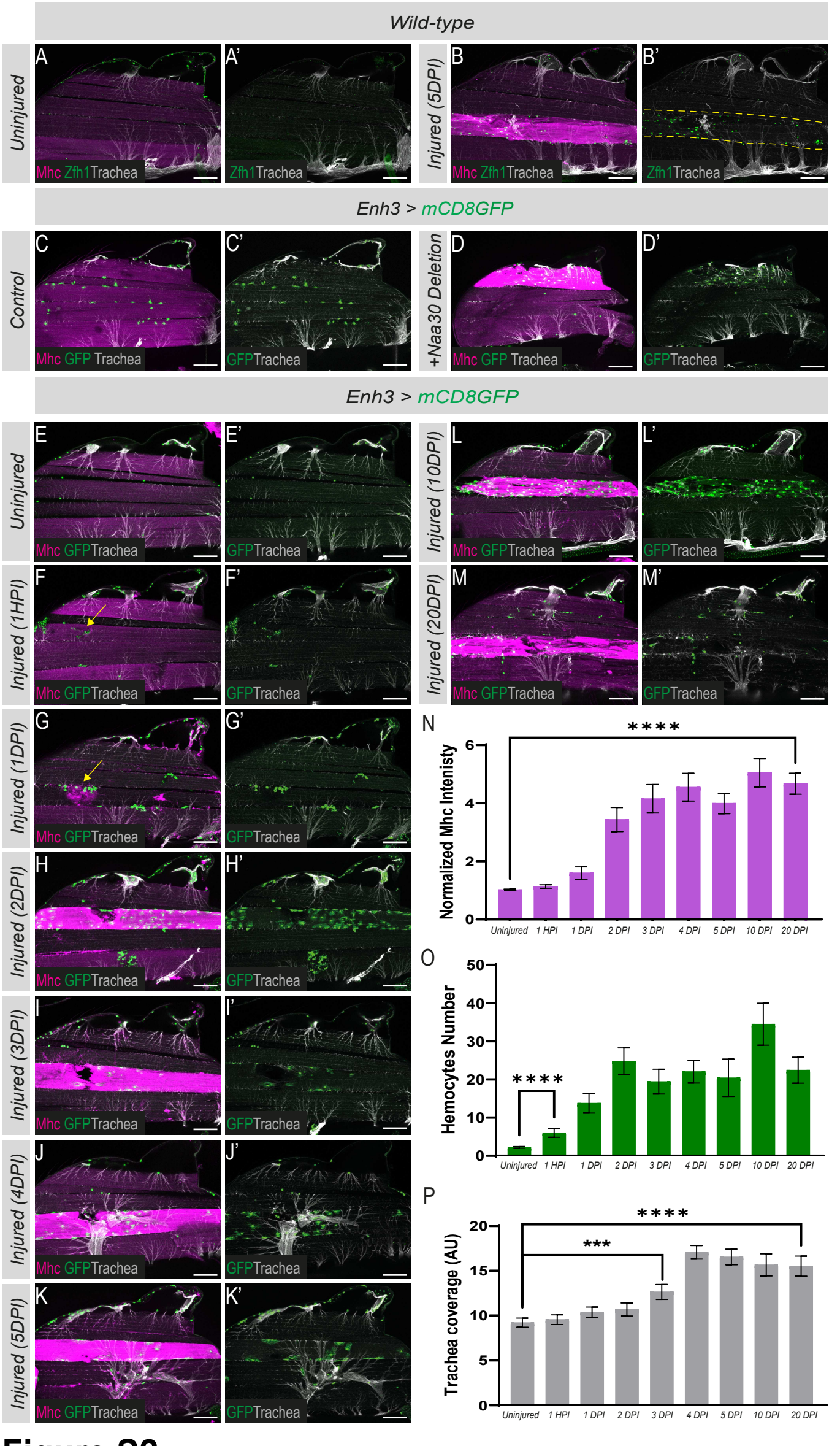
Wild-type
Uninjured
Injured (5DPI)
A
A'
B
B'
Mhc Zfh1 Trachea
Zfh1 Trachea
Enh3 > mCD8GFP
Control
+Naa30 Deletion
C
C'
D
D'
Mhc GFP Trachea
GFP Trachea
Enh3 > mCD8GFP
Uninjured
Injured (10DPI)
Injured (1HPI)
Injured (20DPI)
Injured (1DPI)
Injured (2DPI)
Injured (3DPI)
Injured (4DPI)
Injured (5DPI)
E
E'
L
L'
F
F'
M
M'
G
G'
H
H'
I
I'
J
J'
K
K'
Mhc GFP Trachea
GFP Trachea
N
Normalized Mhc Intenisty
****
0
2
4
6
Uninjured
1 HPI
1 DPI
2 DPI
3 DPI
4 DPI
5 DPI
10 DPI
20 DPI
O
Hemocytes Number
****
0
10
20
30
40
50
Uninjured
1 HPI
1 DPI
2 DPI
3 DPI
4 DPI
5 DPI
10 DPI
20 DPI
P
Trachea coverage (AU)
****
***
0
5
10
15
20
Uninjured
1 HPI
1 DPI
2 DPI
3 DPI
4 DPI
5 DPI
10 DPI
20 DPI

Figure S2

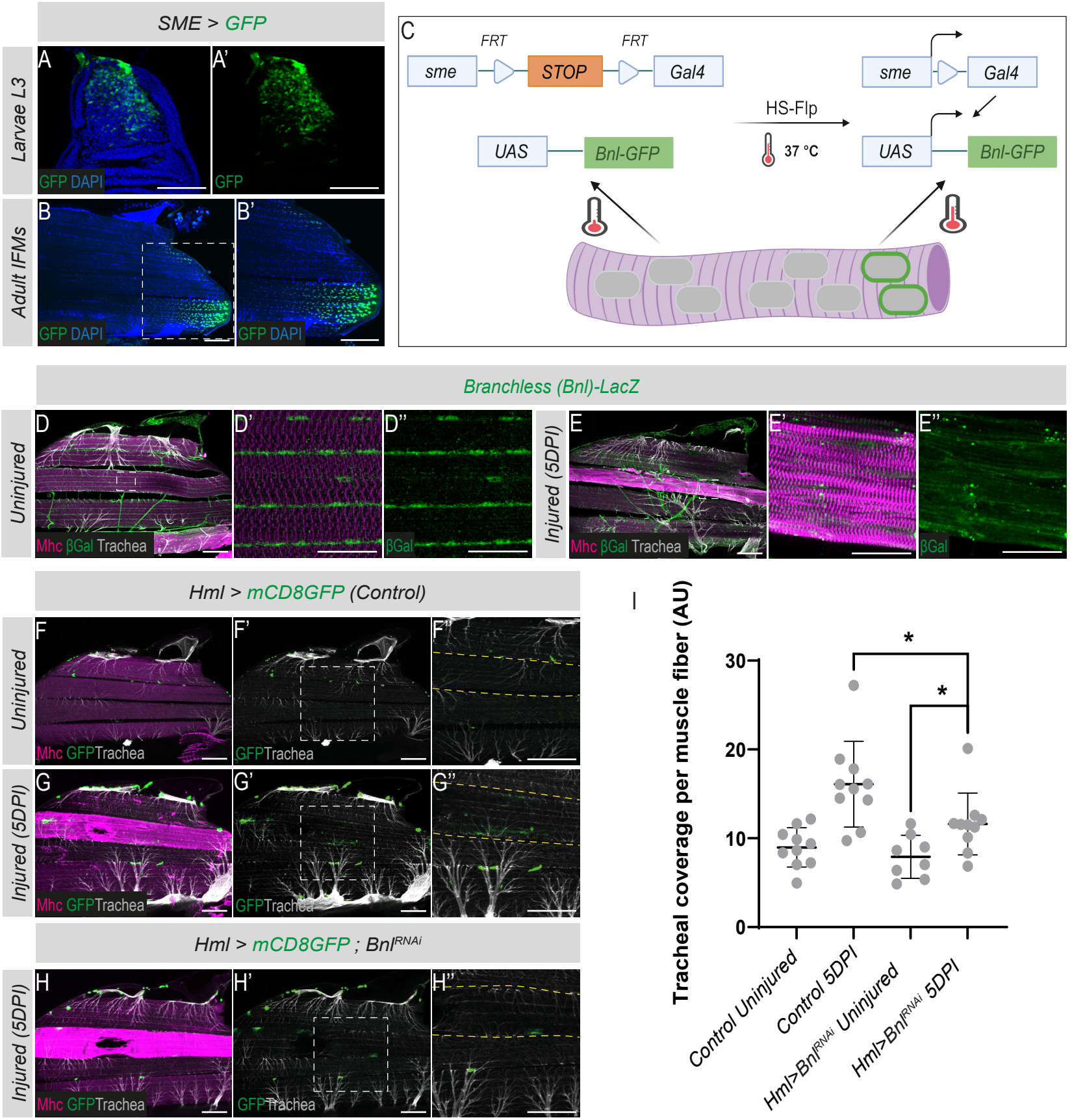
SME > GFP
Larvae L3
Adult IFMs
A
A'
B
B'
GFP DAPI
GFP
C
FRT
FRT
sme
STOP
Gal4
sme
Gal4
HS-Flp
37 °C
UAS
Bnl-GFP
UAS
Bnl-GFP
Branchless (Bnl)-LacZ
Uninjured
Injured (5DPI)
D
D'
D''
E
E'
E''
Mhc βGal Trachea
βGal
Hml > mCD8GFP (Control)
F
F'
F''
G
G'
G''
Mhc GFP Trachea
GFP Trachea
Hml > mCD8GFP ; Bnl^RNAi
H
H'
H''
I
Tracheal coverage per muscle fiber (AU)
30
20
10
0
*
*
Control Uninjured
Control 5DPI
Hml>Bnl^RNAi Uninjured
Hml>Bnl^RNAi 5DPI

Figure S3